In-Space Additive Manufacturing: A Review

Miguel Hoffmann
Wm Michael Barnes 64 Department of Industrial and Systems Engineering,
Texas A & M University,
College Station, TX 77840-3131
e-mail: miguelh18@tamu.edu

Alaa Elwany[1]
Wm Michael Barnes 64 Department of Industrial and Systems Engineering,
Texas A & M University,
College Station, TX 77840-3131
e-mail: elwany@tamu.edu

Manufacturing or repairing parts on-site, high geometric freedom, and feedstock efficiency have long been regarded as nascent capabilities of additive manufacturing (AM) technologies. Researchers aim to adopt these capabilities for the future of space exploration, and polymer AM demonstrations in space were achieved in 2014; however, methods to process metals and other materials are needed. This paper provides a comprehensive review of AM research tested on reduced-gravity platforms from academia and industry across the globe. In addition, complementary processes and technologies under development are summarized. Reports from the literature are categorized by established AM process terminology and processed material. Lastly, alternatives to enabling metal AM in space are discussed, and knowledge gaps are presented. [DOI: 10.1115/1.4055603]

Keywords: additive manufacturing, 3D printing, space, gravity, microgravity, direct write, literature review

1 Introduction

The future of space exploration is dependent on technologies that maximize mission endurance and self-sufficiency. As missions venture further away from Earth, resupply logistics fail to accommodate the probability of component failure and uncertainty about which component may fail [1,2]. A promising solution entails integrating repair and fabrication techniques into the space mission, providing on-demand capabilities to adapt to unforeseen situations. These techniques take various forms to accommodate different space environments and are collectively referred to as in-space manufacturing (ISM).

To discuss the state-of-the-art, we differentiate ISM from terrestrial space manufacturing based on the gravitational condition where the manufacturing activity, not the product, is employed. Terrestrial or for space manufacturing takes place in 1g, where g is the acceleration created by gravity at Earth's surface, on average 9.81 m s^{-2}. In contrast, ISM is performed in reduced-gravity conditions, including microgravity (μg) during orbital or interplanetary spaceflight and partial gravity (e.g., Lunar or Martian gravity) on planetary surfaces. ISM is further categorized based on three operational scenarios.

1.1 Intravehicular In-Space Manufacturing. Manufacturing inside a pressurized structure, including the platforms, is listed in Table 1. Main challenges include μg effects, process safety, and platform constraints (e.g., limited footprint, power). Applications focus on logistics improvements and the fabrication of replacement parts. The National Aeronautics and Space Administration (NASA) has performed notable work in this area as part of the Marshall Space Flight Center (MSFC) ISM project initiative, which aims to expedite ISM development by granting small business innovative research (SBIR) contracts to companies and universities and facilitating access to μg platforms [14]. Companies that have received SBIR awards include Made In Space Inc (MIS), Techshot Inc., and Tethers Unlimited Inc (TUI).

1.2 Extravehicular In-Space Manufacturing. Manufacturing in the external space environment introduces the challenges of vacuum conditions, extreme temperatures, space debris, and radiation, among others [15,16]. The main developments in this area are being incorporated into NASA's on-orbit servicing, assembly, and manufacturing project [17–19] and include the robotic refueling and servicing of satellites and assembly capabilities of large structures not compatible with launch conditions [20–22]. Additionally, NASA's history of in-space assembly development and potential commercial applications are discussed in Ref. [23].

1.3 Planetary In-Space Manufacturing. Construction of habitats and other large-scale architectures are on planetary surfaces. This area may also be considered a component of in situ resource utilization, which deals with the extraction and use of raw materials (e.g., regolith) [24,25].

Traditional manufacturing techniques such as welding [26] and casting [27, p. 101] were evaluated for ISM in the 1960s era of space exploration. In the late 1990s, researchers began to consider the potential of additive manufacturing (AM) to reduce reliance on spare part inventories, citing more efficient packaging of feedstock materials (compared to subtractive techniques) as a critical benefit [28,29]. The interest grew proportionally as AM capabilities matured, from plastic prototypes to functional metal parts [30,31].

AM, colloquially known as 3D printing, is now predominant within ISM investigations across space agencies and research institutes, including NASA [32,33], the European Space Agency [34], and the Chinese Academy of Sciences (CAS) [35]. We emphasize that in-space additive manufacturing (ISAM) is part of the broader ISM field, and non-additive capabilities, such as subtractive manufacturing, automated post-processing, and assembly, are also required.

Important ISAM milestones were achieved in the last decades (see Table 2), including the first in-space fabrication of a tool [36] and the installation of AM machines aboard the International Space Station (ISS) [33,36–38]. However, there is a degree of ambiguity, and at times exaggeration, about present ISAM capabilities. Additionally, as the scope of ISAM applications continues to grow and similar technologies are envisioned to produce tools within a spacecraft and construct habitats on Mars [39], determining the state-of-art or technology readiness level (TRL) [40] has become increasingly complicated; hence our motivation for conducting this review.

A comprehensive in-space 3D printing report was released in 2014 [41], providing valuable recommendations and insights for future work; however, as shown in Table 2, significant progress has occurred in the last eight years. Numerous articles summarize ISAM applications, benefits, and current challenges [42–45], often focusing on the work performed by a specific space agency. An excellent paper by Sacco and Moon [46] reviews AM for space applications. None of the published articles effectively

[1]Corresponding author.

Manuscript received December 15, 2021; final manuscript received September 3, 2022; published online November 3, 2022. Assoc. Editor: Qiang Huang.

Table 1 AM microgravity research platforms

Platform	Gravity level (g)	μg duration	Examples	References
Drop tower	10^{-6}–10^{-2}	1.3–9.5 s	HITec Einstein-Elevator NASA Glenn Drop Tower	[3–6]
Parabolic flight campaigns	10^{-3}–10^{-2}	15–25 s	Airbus A310 ZERO-G NASA KC-135	[7–9]
Sounding rocket	10^{-5}–10^{-3}	3–20 min	MASER 11 TR-IA-3	[10,11]
Satellite	10^{-6}–10^{-5}	Month-years	International Space Station SJ-10 Recoverable Satellite	[7,12,13]

Table 2 AM processes tested in μg

Year	Process	Material	Platform	Section
1995	MJT	Silicone oil	Sounding rocket	4.2.1
1999	MEX	ABS	PFC	4.1.1
2002	MJT	Aqueous glycerol	PFC	4.2.2
2006	MJT	Aqueous glycerol	Drop tower	4.2.3
2007	DED	Aluminum 2319	PFC	4.4.1
2011	MEX	ABS	PFC	4.1.2
2013	MEX	ABS	PFC	4.1.2
2014	MEX	ABS	ISS	4.1.3
2016	MEX	PLA	ISS	4.1.4
2016	MEX	PLA	PFC	4.1.5
2016	MEX	PLA	PFC	4.1.6
2016	MEX	ABS	ISS	4.1.7
2016	DED	Aluminum alloy	PFC	4.4.2
2018	VPP	Alumina resin	PFC	4.5.1
2019	MEX	ULTEM 9085	ISS	4.1.8
2019	MEX	Biomaterial	ISS	4.1.9
2019	PBF	316L stainless steel	PFC	4.3.1
2019	PBF	Polystyrene	PFC	4.3.2
2020	PBF	Regolith simulant	Drop Tower	4.3.3
2020	MJT	Polystyrene suspension	Satellite	4.2.4

Note: ABS, acrylonitrile butadiene styrene; PLA, polylactic acid; CFR-PLA, carbon fiber-reinforced PLA.

summarize and categorize the growing list of manufacturing technologies tested in μg.

The objectives of this work are (1) to direct readers through the growing list of ISAM publications by grouping them according to established terminology and relevant mission conditions and (2) to reveal currently achievable capabilities and future research needs. The paper starts with overviews of the employed μg research platforms and the AM process chain in Secs. 2 and 3, providing the necessary context and terminology for the rest of the paper. Then, in Sec. 4, we conduct a comprehensive review of the literature studies that tested AM technologies in μg conditions, grouping them based on the established process category standards. The publications reviewed are most directly applicable to intravehicular ISM scenarios. Several AM variants have been explored for planetary and extravehicular ISM; however, we limit our coverage of these studies to a few notable examples due to their lack of validation under μg. In Sec. 5, we summarize complementary manufacturing technologies validated in reduced-gravity platforms and ISM technologies under development. In Sec. 6, we present two categorizations of the cited studies by AM process category and type of processed material. Lastly, Sec. 7 discusses knowledge gaps and future research needs.

2 Microgravity Research Platforms

Perfect weightlessness (i.e., "0g") is an ideal state that is only achievable for a few seconds in space [7]. In practice, the level of weightlessness is altered by residual acceleration and vibrations (i.e., g-jitters) [47]. Therefore, "microgravity" (μg) is a more accurate term to indicate that g, i.e., the acceleration of weightiness created by gravity at Earth's surface, is "very small." Experienced μg levels vary between 10^{-3} and $10^{-6}g$, depending on the research platform (see Table 1) and experimental conditions.

Examples of ground-based (i.e., non-orbiting) μg facilities include drop towers [3–6], balloon drops [48], magnetic levitation-based simulators [49], aircraft parabolic flight campaigns (PFCs) [7,8], and sounding rockets [10]. Orbiting μg platforms include CubeSats [50], recoverable satellites [12], and the ISS [13]. When comparing μg platforms for AM experiments (Table 1), the researcher needs to consider the continuous μg period, the associated transient accelerations, the number of tests, and any design (e.g., mass, footprint) or safety constraints the experimental payload must accommodate. Below we briefly describe the μg facilities employed for the AM studies discussed in Sec. 4. The interested reader can refer to Refs. [7,11,48] for more details on these and other μg research platforms.

2.1 Drop Tower. A drop tower is a vertical shaft that provides microgravity levels between 10^{-6} and $10^{-2}g$. Modern drop towers (e.g., the Einstein-elevator) accommodate experimental loads with a mass of up to 1000 kg, dimensions of 1.7 by 2 m, and up to 300 tests per day [4]. Other advantages of drop towers include their relatively low cost, accessibility, and the possibility to implement vacuum conditions. Their main drawback is the limited μg duration, ranging from 1.3 to 9.5 s based on the tower's height, and the significant transient accelerations (up to 50g) during the loading and breaking phases [11].

2.2 Parabolic Flight Campaigns. Modified aircraft (e.g., Boeing 727–200, Airbus A310) can provide 10^{-3}–$10^{-2}g$ levels of μg by performing aerobatic maneuvers (Fig. 1) known as parabolas. The procedure begins with the aircraft reaching a starting altitude of 7.0–8.6 km above sea level and then flying horizontally. Subsequently, a typical parabola maneuver starts with the plane rapidly ascending at 45 deg (i.e., pull-up), tracing a parabolic arc pattern (i.e., pushover) at 7.3–10.4 km altitudes, and descending at 45 deg (i.e., pull-out), transferring the rapid descent into a horizontal steady flight phase. The parabola maneuver is repeated 30–40 times in succession or with short breaks, requiring 2–3 h of total flight time. PFCs usually consist of three to four flight days [9,11,51].

Each parabola maneuver provides ~22 s of μg, preceded and followed by ~25 s of transient accelerations (1.5–2.5g) during the pull-up and pull-out segments [11,51]. The parabolic arc pattern during pushover can be adjusted to provide ~30 s of Lunar gravity (i.e., 0.16g) or ~40 s of Martian gravity (i.e., 0.38g) [9]. PFCs are commonly used to validate technical hardware and operational and experimental procedures and to train ISS crews. Their primary advantages are that the AM researcher may be present during the experiments for manual interventions and in situ observations, and large (up to 2.9 m in height, several tons in weight) experimental loads can be accommodated. However, the μg duration is still inadequate for 3D printing samples, the μg level is relatively low, and the hypergravity phases may affect final conclusions [11,51].

2.3 Sounding Rocket. Sounding rocket flights provide μg levels of 10^{-5}–$10^{-3}g$ for automated or remotely operated

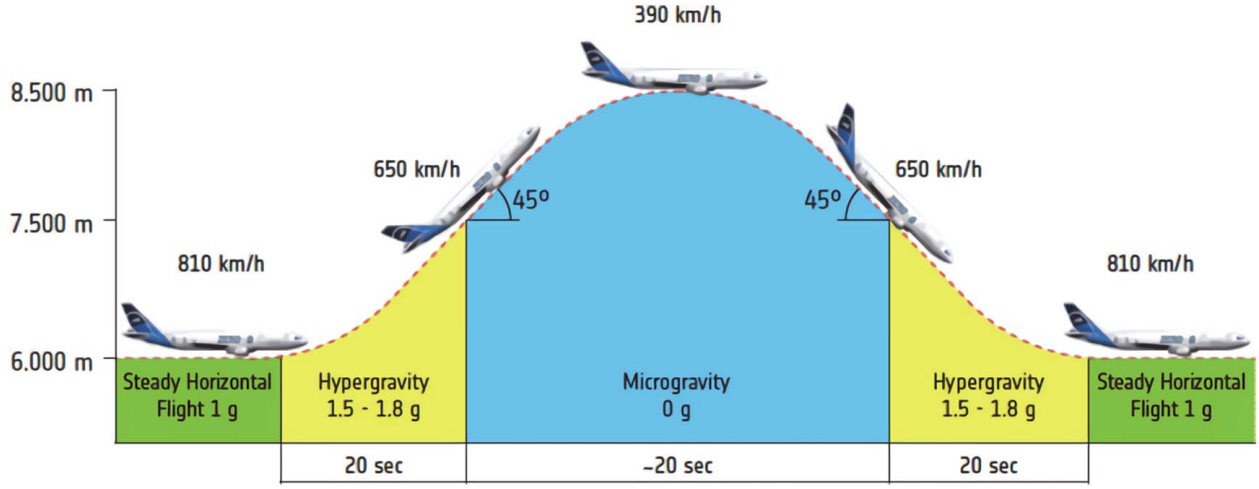

Fig. 1 Parabolic flight maneuver of the Airbus A310 Zero-G [51]

experiments [7, ch. 1]. These rockets reach altitudes of 250–350 km from which the experimental payload is released, undergo free-fall, and land by parachute. The free-fall phase lasts 3–20 min, depending on the rocket's size, engine, and maximum altitude. These factors also determine the possible payload footprints. Since they are unmanned, payload safety requirements are less stringent than PFCs [7,11]. We are aware of only one AM study in μg (Sec. 4.2.1) that employed sounding rockets.

2.4 Satellite. Satellites represent the only μg research mediums that can provide sufficient time for samples to be 3D printed in μg without introducing hypergravity phase concerns. However, missions using orbital platforms require long preparation, typically several years [7].

2.4.1 Recoverable Satellite. Recoverable satellites such as the SJ-10 [12] can provide several months of μg, at levels as low as $10^{-5}g$, in addition to vacuum conditions, and are an attractive alternative for countries without access to the ISS. These satellites orbit the Earth at altitudes of ~500 km and include the necessary capabilities (e.g., power, telemetry, telecommand) to conduct experiments remotely. Several payloads are included simultaneously and may only be retrieved upon satellite recovery at the end of the mission [48]. We are aware of only one AM study in μg (Sec. 4.2.4) that employed recoverable satellites.

2.4.2 International Space Station. The ISS orbits the Earth at 400–450 km altitudes and is currently the only manned μg research platform for long-duration (months to years) studies [13]. The μg level is 10^{-6}–$10^{-5}g$, depending on internal perturbations (e.g., crew movements) and vibrations [7,11]. However, access to the ISS is minimal, and several aspects restrict potential AM payloads. First, the experimental payload is restrained by capacity limitations aboard the ISS and constraints in the "up mass" and "down mass" when launching and returning the AM machine or samples. Second, the payload must comply with ISS environmental prerequisites; thus, it must provide adequate containment levels, outgassing prevention, and other safety requirements. Lastly, the experimental procedures should be automated or teleoperable to reduce dependence on the limited astronaut time [11].

3 Additive Manufacturing Overview

The capabilities of AM have improved dramatically in the last decade, permitting its use across many industries, such as the aerospace, automotive, and biomedical industries [52–55]; however, limitations, many of which are exacerbated when translating AM systems into space, remain. This section intends to provide readers unfamiliar with AM with the basic terminology and context for the subsequent sections. Additionally, it addresses some of the common AM misconceptions and illustrates the auxiliary technologies needed to achieve the full potential of ISAM.

The ISO/ASTM 52900 standard describes AM as "the process of joining materials to make parts from 3D model data, usually layer upon layer" [56] and defines seven distinct process categories: material extrusion (MEX), powder bed fusion (PBF), directed energy deposition (DED), vat photopolymerization (VPP), material jetting (MJT), binder jetting (BJT), and sheet lamination (SHL) processes [56]. A part is fabricated layer-by-layer in all AM processes, following directions derived from a digitized geometry. Technologies are differentiated by how layers are created, how the layers are bonded together, and the type (e.g., polymer, metal, ceramic) and form (e.g., powder, wire, liquid) of feedstock that can be processed. These differences will regulate critical factors of the printed part, such as mechanical properties, geometrical accuracy, degree of post-processing needed, and the overall manufacturing system footprint. Most AM systems employ 3D Cartesian motion architectures, but alternatives such as robotic arms [57,58], delta [59], and polar systems [60] are available. AM can simplify the production of artifacts with complex geometries without additional tooling or fixtures, leading to its association with terms like *direct manufacturing*. However, substantial work is needed before AM becomes the simple "push button" process that the media have hyped. AM machines seldom directly produce ready-to-use parts; pre- and post-processing steps are commonly required [61–63]. Some of these steps can be easily automated or addressed via teleoperation; others represent key challenges to ISAM.

(1) *3D Model Generation*. The process starts with the generation of a computer-aided design (CAD) model of the part to be printed. This digital model contains the necessary 3D data to fully describe the part's geometry and is commonly obtained using CAD modeling software or reverse-engineering methods such as 3D scanning.
(2) *3D Model Conversion Into AM Machine Format*. Most AM technologies accept the .stl file format, which approximates the surfaces of the 3D model using triangular facets and is commonly obtained automatically from the software used in step one. The .amf file format is becoming a prevalent alternative to .stl files, as it includes additional part information (e.g., material and color). The file format conversion might introduce errors, such as gaps or undefined geometries, which will likely prevent the part from being built as intended. Minor errors are usually fixed automatically with the slicer used in step three. Complex errors typically encountered if low-fidelity scanning methods were employed in step one require the use of specialized .stl/.amf repair software.

(3) *Transfer File to AM Machine and Manipulation*. Once generated (and repaired if needed), the .stl/.amf file is transferred to the AM machine's slicer, i.e., the software used to convert the model into commands (e.g., G-code) the AM machine understands. The slicer is used for at least one of the following functions: (1) specify the layer thickness, (2) define the proper orientation and location of the part with respect to the build plate, (3) scale the model to account for process shrinkage or subsequent machining operations, and if required, (4) generate support structures. Some AM machines employ the slicer to specify all process parameters, while others may require multiple software packages.
(4) *Build Preparation*. This can be divided into two groups: process parameters and physical setup. Process parameters are highly machine-specific and are related to the method used to fuse the materials, the building speed, and many other factors. Physical setup includes cleaning the machine from previous prints, loading the required feedstock, calibrating the device, and ensuring that build settings (e.g., gas pressure) are within the required values. The physical setup is typically performed manually and can be time-consuming and labor-intensive.
(5) *Part Building*. This is where the layer-based manufacturing process occurs, mostly automatically. While extensive research efforts on process monitoring and control aim to detect process errors automatically [64–66], manual supervision at regular printing intervals remains a common practice.
(6) *Part Removal*. Once printed, the built part must either be retrieved from surrounding material, detached from the build platform, or both. Depending on the AM technology, this step may require supporting equipment ranging from simple hand tools to wire electric discharge machining. For instance, simple plastic parts built via MEX may be printed without support structures, and their bond with the build platform is often sufficiently weak, such that they can be separated by hand or using a spatula. In contrast, metal parts built via PBF are entirely enclosed by loose powder and welded onto the build plate, requiring brushes, wet vacuum cleaners, and machining equipment.
(7) *Post-Processing*. This step is highly dependent on the AM technology used and the finished part's requirements (e.g., surface roughness, dimensional tolerance, mechanical properties). It ranges from simple part cleaning to complex processing such as heat treatments and computer numerical control (CNC) machining, which can substantially increase the overall footprint of the needed hardware and operator involvement. Recent papers [67–69] have demonstrated potential approaches to simplify post-processing steps, but a degree of manual labor, often substantial for metals, remains the norm.
(8) *Quality and Analytics*. AM employs destructive and nondestructive methods to evaluate the quality of the manufactured artifacts. Destructive methods are mainly used to determine mechanical properties and include tensile [70], flexural [71], and compression testing [72]. Non-destructive evaluation includes visual and photographic inspection, optical and scanning electron microscopy analysis, structured light scanning, three-dimensional computed tomography, and density calculations [73].

Robot-assisted AM is an emergent field that could reduce human involvement in the AM process chain and provide the pathway toward a fully teleoperable or even autonomous ISAM system. Future ISAM systems could integrate robotic agents in two ways: (1) a robotic agent, independent of the AM machine, could perform tasks such as loading the feedstock and translating the part from AM to machining subsystem, or (2) the robotic agent is internal to the AM process, performing both AM and post-processing within a single system, as shown in Ref. [74]. Most applications of robot-assisted AM in the literature do not use robotic agents to simplify pre- or post-processing steps; instead, most cases show the use of robot arms with six degrees-of-freedom to replace the traditional motion system (i.e., Cartesian), intending to achieve multidirectional manufacturing, conformal deposition, and large-scale AM [75,76]. This approach has been demonstrated with MEX [77,78], DED [79–81], and VPP [82–84].

3.1 Direct Versus Indirect Additive Manufacturing. Technologies from each of the seven AM categories have evolved to be capable of processing feedstock from polymers, metals, and ceramics; however, achievable properties (e.g., mechanical, geometric) and supporting infrastructure (e.g., furnaces, milling) differ significantly. The industry's most established metal AM processes, PBF and DED, can process feedstock *directly*, meaning no sacrificial materials (e.g., polymer binders) are involved and are heavily used in the aerospace industry [53]. Despite the relative maturity of PBF and DED processes, achieving high-quality parts that account for anisotropic microstructures and potential defects requires substantial effort, and fundamental knowledge gaps remain present [85].

AM processes can also produce metal and ceramic parts *indirectly* by following an approach based on powder injection molding, which involves four main steps: (1) mixing of powder (metal or ceramic) with a binder system (35–50 vol%) [86]; (2) injection molding to form a "green" part, i.e., a weak artifact where the binder holds the powder in place; (3) debinding (e.g., pyrolysis, solvent-based) leaving behind a "brown" part, i.e., a porous artifact made up of the powder [87]; and (4) furnace sintering where heat is used to coalesce the powder into a solid mass without melting, resulting in dimensional shrinkage. The binder system may include up to three polymeric materials, including the main binder that is removed during the debinding step, a secondary binder that holds together the powder as the main binder is removed, and additives to help disperse the powder in the binder system [88]. AM follows the same four steps but replaces injection molding with its particular method of shape creation and has been demonstrated for MEX [89–92], BJT [93,94], and VPP [95], among others. The geometrical constraints and achievable mechanical properties are typically similar to those in powder injection molding [87].

As discussed in later sections, DED and PBF have been tested in μg platforms, and indirect metal AM methods are under development. Each technique offers unique characteristics, so arguments for and against their feasibility in space must be considered. PBF benefits from substantial industry knowledge [96, p. 133], but large system footprint and safety concerns due to lasers and powders led to the technology mainly being disregarded for ISAM; yet μg testing via PFC was performed in 2019 (see Sec. 4.3.1). DED can process wire feedstock, which is much easier to handle in μg. Still, the geometric capabilities are limited, power requirements are usually high, and substantial machining, which introduces risks of floating debris, is required. Indirect methods may offer a user-friendly process chain [97], and the fusion mechanism produces uniform microstructures [98]. Still, they also have inherent limitations, both terrestrially and for ISAM. Once the feedstock is formulated, three separate systems are required for the shaping, debinding, and sintering steps. The footprint can be reduced to two systems by performing the debinding step through pyrolysis at the expense of much larger debinding times and geometrical constraints, e.g., parts with sudden thickness variations must be redesigned to avoid distortion and cracking during sintering [99]. Additional challenges include handling toxic fumes and disposing of the binder in μg.

4 Additive Manufacturing Processes in Microgravity

4.1 Material Extrusion Processes. MEX is an ASTM/ISO classification for AM technologies where "material is selectively dispensed through a nozzle or orifice" [56] when pressure is applied while the printhead or build platform moves in a plane.

The process relies on controlling the feedstock material state, achieved using temperature to melt and liquefy material in a reservoir, chemical reactions to cause solidification, or a combination of the two [61, p. 171]. MEX can be classified into three main variants based on the type of extruder mechanism used: (1) filament-based MEX for processing filaments, (2) screw-based MEX for processing pelletized feedstock or highly viscous pastes, and (3) plunger-based MEX for dispensing inks [100]. Filament-based MEX of polymers, referred to as fused filament fabrication (FFF), has been explored extensively under μg conditions and is the main focus of this section.

Screw-based and plunger-based MEX variants are comparable to FFF but replace the gear-based extruders with pump mechanisms to create continuous liquid deposits with a wide range of viscosities [101,102]. We note that some of these technologies may also be classified as direct write (DW) [103,104], a process category not mentioned in the ISO/ASTM 52900 taxonomy [56], that is considered synonymous with AM. Several technology names exist under these MEX variants, often differing only by the processed feedstock. Some of these include colloidal-inks [105], water-based slurries [106], and pastes [107]. The patented SmartPump™ technology (nScrypt Inc) enables the deposition of extrudates with viscosities ranging from 1 cP to 1 million cP [108,109] and has been tested aboard the ISS (see Sec. 4.1.9). Screw-based and plunger-based MEX technologies are also suitable for fabricating large-scale structures, some of which have been investigated for extraterrestrial surface construction [110,111].

The FFF process, also known as fused deposition modeling (FDM) [112], employs a gear-based extruder to feed a continuous thermoplastic filament into a heating chamber where it is liquefied by conduction. As it enters the chamber, the filament acts as a ram that pushes the semi-molten polymer through a nozzle and onto a substrate plate where it solidifies. This material delivery system (i.e., printhead) is installed on a control system that coordinates motion and deposition to produce a predefined layer geometry. Upon completion of the layer, the nozzle is raised (or the build plate is lowered) by a distance matching the specified layer thickness, and the next layer is deposited [113]. Selecting bigger diameter nozzles or increasing layer thicknesses decreases the printing time at the expense of part resolution [114].

When depositing molten thermoplastic, particularly during the first layer, a sufficiently strong bond must be established between the thermoplastic and the substrate to ensure part stability during the rest of the build. Additionally, equalizing temperature differentials is desirable to reduce thermal stresses that may cause warping (i.e., curling). These two requirements are facilitated by building plates or enclosures with heating capabilities and closed-loop positional control for Z-calibration distance [115]. The Z-calibration distance defines the actual Z-value datums across the build surface, permitting the gap between the nozzle orifice and the build plate (i.e., the stand-off distance) to match the specified first-layer thickness as the printhead moves in the *XY* plane. FFF printers typically achieve this with a *Z*-axis sensor to probe multiple XY locations on the build plate and subsequently use that height data to compensate for discrepancies. Indicators that the nozzle orifice is too close to the build surface include extrudates exhibiting ridges, visibly wider first layers, and parts too strongly bonded to the plate. As a result, the part removal postprint becomes strenuous, increasing the likelihood of damaging the part and plate. Furthermore, the stand-off distance can influence the thermal flow, cooling and deposition rates, and interlayer bonding [116].

Several FFF characteristics have permitted its extensive validation in μg conditions, including the safety and simplicity of the process, low machine footprint and power requirements (70 W to 1.4 kW), and reduced risk of material contamination [117–119]. FFF's main drawback is that it can only directly process polymers; common filaments include acrylonitrile butadiene styrene (ABS), polylactic acid (PLA), carbon fiber-reinforced PLA (CFR-PLA), polyetherimide (PEI), polycarbonate (PC), and high-density polyethylene (HDPE) [120]. ULTEM 9085 is a mixture of PEI and PC blend [121] that is certified for use in the automotive, medical, and aerospace fields [122]. To address current polymer limitations, materials with superior mechanical properties (e.g., composites and metallic glasses) were adapted for FFF [123–128]. FFF can also indirectly process metals and ceramics [97,129,130]. Metal FFF, also known as bound metal deposition (BMD) in the literature, is a candidate technology for metal ISAM aboard the ISS [131] and is discussed further in Sec. 5.4.7.

4.1.1 Parabolic Flight Campaigns—Acrylonitrile Butadiene Styrene. In June 1999, Crockett, Petersen, and Cooper performed the first-ever FFF μg studies through PFCs (NASA KC-135 Boeing 707). Two machines were used to process ABS: a commercial FFF machine (FDM 1600, Stratasys Ltd.) and a custom-built deposition system [132].

Prior to the PFCs, the researchers hypothesized that FFF in μg would be successful based on two criteria. First, gravity would not affect the bead shape if the diameter of the FFF bead was below a theoretical maximum dimension derived from the material's capillary limit. The diameter of FFF beads is approximately equal to the nozzle orifice (typically 0.1–1 mm), so this condition should be met. Second, ensuring a continuous substrate (the previous layer) is provided by depositing layers with a slenderness ratio below a height limit approximately equal to the circumference of the bead. Furthermore, the researchers mentioned that in 1g, larger-than-optimal layer heights might create minor gaps or flaws. However, in μg, the flaws would be more severe, thus requiring optimal process parameters to be determined. The researchers initially tested the hypothesis on the ground by printing objects perpendicular and opposite to gravity by placing the commercial FFF machine on its side and upside down, respectively, and concluded that, at least visually, the objects were identical to replicas built in the standard orientation [132].

The PFCs included four flights, providing 40 parabolic arc flight paths per flight and a total of 1 h and 20 min of μg printing time [133]. Overall, 14 ABS specimens in seven different geometries were manufactured. The geometries were selected to analyze interlayer and intralayer bonding, support structure requirements, and dimensional stability compared to replicas printed in 1g. The researchers [132] concluded that FFF appeared to be a feasible manufacturing technique for μg environments, with visible results appearing almost identical in μg as in 1g. Additionally, they stated that reduced gravity could reduce the need for support structures. However, they declared two experimental limitations of the PFCs: the effects of different gravity regimens during aircraft pull-out and the effects of atmospheric humidity on the ABS feedstock.

Cooper and Griffin prepared a technical memorandum [134] that documented the hardware used for the PFCs and provided the requirements for a potential ISS flight configuration. In Ref. [135], Cooper et al. illustrated the advantages of installing a polymer AM device onboard the ISS through four types of scenarios: (1) predicted repairs to extend the life of components and obtain logistics savings; (2) production of experimental hardware to reduce constraints caused by launch requirements; (3) unknown repair and replacement; and (4) provide novel experimentation and educational advantages.

4.1.2 Parabolic Flight Campaigns—Acrylonitrile Butadiene Styrene. In 2011 and 2013, MIS verified and extended the work by NASA researchers through PFCs (Zero-G Corporation—Boeing 727), focusing on assessing FFF machine functionality in μg and determining the correlation between gravity levels (μg, 0.16g, and 0.38g) and specimen layer thickness [136].

Three FFF machines were used to process ABS: a BFB 3000 (3D Systems Inc.), a Thing-O-Matic (MakerBot Industries LLC), and an MIS custom-built printer. The MIS team [136] reported that several mechanisms of the two commercial printers malfunctioned during initial μg trials, requiring "a large amount of modifications" to

print normally during the tests; however, specific malfunctions or subsequent modifications are not described.

The g-level versus average layer thickness correlations were derived by printing columns (only with the BFB 3000 machine) during the reduced-gravity portion of the flights and measuring their respective layer thicknesses via optical microscopy. The average layer thicknesses produced during the three reduced-gravity regimes were equivalent to those obtained in 1g, with minor differences attributed to errors in measurement. Unfortunately, the employed process parameters, column dimensions, and the number of printed specimens are not reported. The authors stated that these studies enabled μg-based FFF to reach a TRL-6 [136].

4.1.3 International Space Station—Acrylonitrile Butadiene Styrene. In September 2014, the 3D printing in Zero-G Technology Demonstration (3DPrint) FFF printer from MIS was launched to the ISS, becoming the first-ever space-based AM device. The 3DPrint device (see Table 3 for specifications) was designed to be operated within the ISS's Microgravity Science Glovebox (MSG), which supplies power to the printer and provides the required level of containment [140]. Similar to commercial FFF devices, albeit with a ruggedized enclosure, 3DPrint processes 1.75 mm diameter filament (ABS) with a heated (230–250 °C) deposition extruder and a 0.4 mm nozzle [37]. However, the 3DPrint device lacked two crucial features: (1) no build plate or enclosure heating capabilities, likely to meet MSG constraints, and (2) no automated closed-loop positional control to calibrate the stand-off distance, relying instead on visual feedback [116]. Details on the MSG and its capabilities are available in Refs. [141,142].

The first uplinked tool, a ratchet wrench, was manufactured in space in December. The digital blueprints of previous prints were available on an SD card launched with the printer. In contrast, the wrench's digital blueprints were sent from the ground. Although a simple 4.48 by 1.29 in. tool, the ABS wrench illustrated how ISAM capabilities could be an asset for future space missions.

The 3DPrint mission goals are summarized in Refs. [133,140], and details on the geometries and dimensions of the printed artifacts are shown in Ref. [37]. 3DPrint specimens were fabricated aboard the ISS in two phases and evaluated terrestrially, hence the significant delays between printing, evaluations, and results publication. Phase I occurred between November and December 2014 [143,144], and phase II occurred between June 28 and July 12, 2016 [145].

Comparisons were made by printing equivalent samples in 1g via a 3DPrint replica unit. Evaluations by Prater et al. [146] included mass, density, mechanical (tensile and compressive) properties, structured light scanning, X-ray computed tomography, surface metrology, Fourier transfer infrared spectroscopy, and scanning electron microscopy analysis. Prater et al. [146] concluded that μg had no engineering-significant effects on FFF based on the experimental results and μg-based material modeling simulations. However, they noted that limited sample sizes and significant build-to-build variability may have masked the effects of μg conditions [116,146].

The extensive build-to-build variability is attributed to the two hardware limitations listed above. In 1g, ABS is almost exclusively printed with a heated bed set to 110 °C (the glass transition temperature) [147] or a heated enclosure [148, p. 223] to minimize warping and delamination defects. We postulate that the lack of a heated substrate was compensated by increasing the Z-calibration distance (i.e., decreasing the stand-off distance) to promote interlayer bonding and minimize warping defects. The artifacts printed with the 3DPrint device [144] showed typical indicators (e.g., ridges, wider first layers, residual material accumulation on the build plates) that the nozzle orifice was too close to the build surface. During phase I, the Z-calibration distance was constant (2.20 mm) for ground prints and variable (2.39–2.84 mm) for each μg print [116]. Considering that the nominal layer thickness is 0.2 mm for a 0.4 mm diameter nozzle, the 0.19–0.64 mm gap changes represent a notable difference in FFF processing conditions. The second-generation FFF printer from MIS (Sec. 4.1.7) addressed these hardware limitations.

4.1.4 International Space Station—Polylactic Acid. In February 2016, the first European in-space AM experiment took place with the testing of the Portable on Board 3D Printer (P_3DP), another FFF device, aboard the ISS. The P_3DP experiment was funded by the Italian Space Agency and marked that the first time PLA was printed in a long-duration μg environment [137]. The P_3DP payload was neither designed nor certified to allow the crew to remove the printed object nor perform the setup for another print run. Instead, the plan was for the P_3DP experiment to fabricate a single PLA Y-pipe joiner aboard the ISS, and following the machine's return to the ground, part removal and testing would occur. P_3DP specifications are listed in Table 3. Planned ground testing included determining density, surface roughness, defects, porosity, hardness, and elastic modulus and how these properties differ from those of a terrestrially fabricated replica [137]. The results of these tests are currently unavailable in the literature.

4.1.5 Parabolic Flight Campaigns—CFR-PLA. According to Ref. [149], in March 2016, CAS researchers conducted FFF μg experiments via PFCs, with CFR-PLA as the feedstock material. Reference [149] states that μg printed samples were compared with 1g-printed replicas. Based on X-ray computed tomography analysis, μg appears to have increased internal porosity and caused periodic sagging at the samples' corners. Unfortunately, we have found no primary sources for this study.

4.1.6 Parabolic Flight Campaigns—Polylactic Acid. In March 2016, Cowley et al. [150] investigated the effects of variable gravity conditions on the FFF processing of PLA filament via PFCs. The researchers used a Replicator II (MakerBot Industries, LLC), with no mechanical or electrical modifications, to print three tensile specimens, two compression specimens, and two print quality specimens during gravity conditions ranging from μg to 2g, i.e., printing was continuous throughout the flight.

The Replicator II is limited to PLA filament processing since it does not include a heated build plate to support first-layer adhesion [151]. Compared to ABS, a heated plate is not essential for PLA due to its lower glass transition temperature [147,151]. The samples produced during the PFCs were evaluated against reference samples printed in 1g. Evaluations included optical microscopy, computed tomography, SEM analysis, tensile testing per ASTM D638-02A [70], and compressive testing per ASTM D695-02A [72].

Table 3 Specifications of FFF devices tested aboard the ISS [137–139]

Attribute	3DPrint	P_3DP	AMF
Dimensions (mm)	330 × 300 × 360	250 × 250 × 250	566.5 × 460.4 × 273.2
Print volume (mm)	60 × 120 × 60	50 × 50 × 45	140 × 100 × 100
Mass (kg)	20	5.4	45
Resolution (mm)	0.35	–	0.15
Power (W)	176	70	600
Material capabilities	ABS	PLA	ABS, HDPE, ULTEM 9085

Optical microscopy and computed tomography indicated that the layers partly or wholly extruded during the varying gravity phases of the flights showed more deformation and bulging than layers extruded in 1*g*. Based on SEM analysis, the swelling corresponded to the extrudate increasing up to 67% in diameter. Interestingly, the extrudate width decreased during the hypergravity portions of the flight and increased during the μg phase (approximately 22 s). The researchers [150] provide several possible explanations for these observations, including (1) hypergravity temporarily changing the build plate to nozzle distance, (2) hypergravity having an impact on the filament feeding system that could influence the feed rate and hence the polymer flow, and (3) the die swelling phenomenon [152].

The mechanical properties are tabulated in Table 4. The authors stated that the values are reasonably consistent regardless of gravity level but highlighted that the compressive specimens fractured at the swollen regions printed during the varying *g* phases of the flight. The researchers concluded that FFF is compatible with μg to 2*g* gravity loads, and specific FFF parameters could be identified to mitigate imperfections during the AM process.

4.1.7 International Space Station—Acrylonitrile Butadiene Styrene. In April 2016, MIS's Additive Manufacturing Facility (AMF) was installed within an ISS EXPRESS Rack [153,154], offering several improvements over 3DPrint (see Table 3). Unlike 3DPrint, which must first be installed inside the MSG, thus requiring careful scheduling ahead of time due to the many other experiments that require MSG access, AMF is more accessible to researchers, only requiring astronaut involvement to load filament feedstocks and remove printed parts. Details on the EXPRESS Rack facilities available at the ISS are available in Refs. [155,156]. Additional AMF upgrades over 3DPrint include a heated substrate and print volume, automated substrate leveling, and calibration, a modified build surface to achieve a better balance between print adherence and ease of removal, changes to maintenance procedures to reduce required crew time, and the capability to process HDPE and ULTEM 9085 [33,138].

Thomas et al. [157] from MIS compared the tensile, compressive, and flexural properties of ABS processed with the AMF aboard the ISS to an AMF ground test unit. The results are summarized in Table 5. Compared to 3DPrint, μg and 1*g* samples produced by AMF were found to deliver less variant mechanical performance in tension, flexure, and compression compared to the 3DPrint experimental samples (Sec. 4.1.3). Furthermore, the strength in tension and flexure of AM parts produced by AMF is up to 27% improved over 3DPrint [157].

Table 4 PLA mechanical properties processed via FFF in varying *g*-levels and 1*g* [150]

Mechanical test	Tensile		Compressive	
Gravity level	Var	1*g*	Var	1*g*
Yield strength (MPa)	33.1	36.6	39.2	42.23
Young's modulus (GPa)	1.23	1.12	1.38	1.33
Ultimate strength (MPa)	33.6	40.2	43.2	47.1

Table 5 ABS mechanical properties processed by AMF in μg and 1*g* [157]

Mechanical test	Tensile ASTM D638		Compressive ASTM D695		Flexural ASTM D790	
Specimens	5	10	4	10	4	10
Gravity level	μg	1*g*	μg	1*g*	μg	1*g*
Yield strength (MPa)	37.8	37.7	48.7	48.9	54.8	57.7
Young's modulus (GPa)	2.091	2.155	1.655	1.505	1.907	2.120
Ultimate strength (MPa)	38.0	37.8	51.1	52.9	58.9	62.3
Ultimate strain (%)	1.8	1.7	4.5	5.4	5.4	5.3

Reference [158] reports that three ISS functional parts were produced using the AMF system: a tow hitch to join two spheres from the synchronized position hold engage and reorient payload, used to evaluate guidance, navigation, and control algorithms in μg on the ISS; an adapter that mounts a velociCalc probe to monitor airflow and health of the oxygen generation system, a critical piece of environmental control and life support hardware on station; and an enclosure for the Bigelow expandable activity modules. MIS and NanoRacks LLC seek to enable on-demand CubeSat deployment capabilities from the ISS. MIS will employ the AMF to print a plastic frame, NanoRacks, LLC, will supply the remaining components (e.g., batteries and sensors), and an astronaut will perform the assembly [138,159]. AMF continues to assist with ongoing material characterization efforts [160] and is attributed to space-based polymeric AM reaching a TRL-9 [161]. Lessons learned through 3DPrint and AMF will aid MIS's ISM technologies under development, such as the Vulcan project discussed in Sec. 5.4.4 and the extravehicular ISM project known as Archinaut [162,163]. It should be mentioned that despite the high TRL reached, MIS's AMF does not permit the use of support structures [138]; thus, only a subset of FFF geometrical capabilities is available in space. Furthermore, no studies on processing HDPE or ULTEM 9085 via the AMF are available.

4.1.8 International Space Station—ULTEM 9085. In February 2019, TUI's Refabricator, an integrated FFF printer and recycler, was installed in the ISS, demonstrating a closed-loop manufacturing process for long-duration missions [154]. The Refabricator utilizes positrusion, a recycling method developed by TUI. It accepts arbitrarily shaped polymer scraps as input material, dries and degases them, and melts and extrudes them through a die, producing the recycled polymer as filament. The cross-sectional dimensions and feed rate of the cooling extrudate are controlled in a continuous analog of closed-die molding [164]. Furthermore, positrusion does not require grinding of the input material, which would compromise the strength of recycled polymers, and therefore could be capable of recycling the same polymers multiple times [165].

The goals of the Refabrication mission included the assessment of ULTEM 9085 recycling in μg, analysis of part degradation based on use and number of recycling cycles, and extension of feedstock contamination due to positrusion [166,167]. Reference [154] mentions that the Refabricator's technology could also be helpful for earth-based recycling applications, such as turning used plastic bags and bottles into high-quality 3D printing filament feedstock. Edmunson et al. [168] mentioned that abnormal recycler operations were reported in Fall 2019, limiting the Refabricator to printing with filament that was recycled on the ground and that the device will return to the ground for analysis, repair, and future re-launch.

4.1.9 International Space Station—Biomaterial. The 3D BioFabrication Facility, developed by Techshot Inc. and nScrypt Inc., was delivered to the ISS in July 2019, with earlier μg testing via PFC conducted in June 2016 [169]. No publications on these μg studies have been found in the literature. However, the Techshot Inc. patents [170,171] describe some of the 3D BioFabrication Facility capabilities, which include the SmartPump™ technology described earlier.

4.2 Material Jetting. MJT, also known as inkjet deposition, includes AM technologies "in which droplets of feedstock material are selectively deposited" [56] from a printhead. The printhead may consist of several nozzles or orifices and employs one of various modes to transform the feedstock from a continuous liquid volume into small discrete droplets. Three of these modes include continuous inkjet (CIJ) droplet formation, drop-on-demand droplet formation, and electrohydrodynamic jet printing [61,

p. 203] [148, p. 269]. MJT techniques are indifferentiable from inkjet-based DW technologies [103,104].

Materials processing in MJT is traditionally limited to a viscosity threshold of 20–40 mPa s, hence the typical use of waxy polymers, acrylate photopolymers, and colloids containing nanoparticles. In these cases, deposited layers are exposed to ultraviolet light to promote polymerization or a heat source to promote solvent evaporation. Low melting point metals (e.g., aluminum, tin, solders) have also been processed via MJT, hence the interest in this technology for in-space electronics repair (see Sec. 5.6).

CIJ systems apply pressure to the fluid reservoir to eject a continuous stream of drops from the printhead's nozzle. Soon after departing the nozzle, the stream breaks into droplets due to Rayleigh instability. The droplets are electrostatically charged and passed through a deflection field to guide their placement onto a substrate or a material container (i.e., a droplet catcher) if they are not part of the build [61, p. 203] [148, p. 269]. In drop-on-demand, pressure pulses created by thermal (bubble-jet) or piezoelectric actuators enable individual jets to exit directly from the nozzle. As the detached jet moves toward the substrate, surface tension pulls the liquid jet into a single spherical drop [172]. Lastly, in electrohydrodynamic jet printing (also called electrospray printing), drops and jets are drawn from liquid surfaces by employing an electric field [172]. The electric field is generated by applying a voltage between a nozzle or needle and a conducting substrate to create electrohydrodynamic phenomena that drive the flow of fluid inks out of a nozzle or needle [173].

In MJT, the final form of the jet is ideally a single drop; however, a large drop along with smaller satellite drops is typical [172]. In general, CIJ systems generate droplets of about 150 μm, almost twice the diameter of the undisturbed jet [61]. Drop-on-demand methods deposit droplets approximately the same size as the orifice, usually tens of micrometers [174]. Electrohydrodynamic jet printing has deposited droplets as small as 0.49 μm with 0.5 μm nozzles [173]. However, nozzle clogging is more likely to occur when small diameter nozzles are employed and, due to their rapid deceleration, the precise placement of smaller droplets is more difficult [174].

MJT challenges beyond droplet formation include control of droplet flight path, the impact of the liquid droplet on a substrate, and the phase change that transforms the liquid into a solid. Therefore, MJT outcomes are influenced by the surface tension and viscosity of the fluid, the droplet's initial mass and velocity, substrate characteristics, and phase changes [172].

4.2.1 Sounding Rocket—Silicon Oil. In 1995, Haga et al. [175] investigated the interaction between Marangoni and electrohydrodynamic convections under μg. The experiments were conducted using a sounding rocket (TR-IA-3) launched by the National Space Development Agency of Japan. Silicon oil was used as feedstock to fabricate a 10×15 mm column held between two parallel silicon plates. Temperature and electric potential data were recorded during the seven minutes of μg. The results demonstrated that convection flow could be controlled by manipulating the electric field and temperature gradient directions.

4.2.2 Parabolic Flight Campaigns—Aqueous Glycerol. In 2002, Edwards et al. [176] investigated the effect of reduced-gravity conditions on liquid jet breakup mechanisms and subsequent drop formation dynamics via PFCs (NASA KC-135). A relatively large nozzle of 1.4 mm was used to deposit mixtures of glycerol (20–50%) and water delivered via a peristaltic pump. The researchers identified two types of jetting instabilities present under 1g and μg: (1) convective instability, where droplets are formed due to "pinching" the end of the attached jet, and (2) absolute instability, where drops are formed individually at the nozzle at a lower formation frequency. Furthermore, for liquid jets produced in μg, the droplet forming time is up to three times longer. The jets are up to three times larger in the absolute instability region compared to the convective instability region. Edwards et al. attributed these observations to surface tension becoming the dominant force in the absence of g.

4.2.3 Drop Tower—Aqueous Glycerol. In 2006, Osborne and Steinberg employed the reduced-gravity drop tower operated by the Queensland University of Technology to determine the modes of liquid jetting observed in μg [177]. The drop tower provides two seconds of continuous μg, and 120 tests (i.e., a total of 240 s of μg) were conducted for this study. Aqueous glycerol delivered to a 1 mm diameter nozzle via a peristaltic pump was used as feedstock. The study domain included Reynolds numbers from 54 to 785 and Weber numbers from 0.39 to 7.58.

Three different modes of jetting were observed: (1) jetting, i.e., a long jet supporting a convective instability that produced uniform drops; (2) chaotic dripping, i.e., a non-existing jet that produced drops of various sizes; and (3) quasi-stable growth, where a large mass of fluid accumulated at the nozzle and did not detach. The transition from jetting to chaotic dripping occurred at Weber numbers between 3.517 and 4. The researchers concluded that during chaotic dripping, the inertial force of the fluid entering the formed dropped from the nozzle replaces g-induced stretching as the mechanism for fluid necking.

4.2.4 Satellite—Polystyrene. In 2020, CAS researchers [178] investigated droplet manipulation methods and evaporation-induced deposition of colloids in μg conditions by sending an experimental colloidal printer aboard the SJ-10 satellite. An aqueous polystyrene colloidal suspension (0.1–0.15 wt% concentration, 3 μm particle size), employed as feedstock, was supplied to two hydrophobic needles (0.1 mm inner diameter) at a rate of 11.42 μl/s via an electromagnetic pump. A hydrophilic quartz glass, heated to 40 °C, was used as the substrate to promote droplet wettability and solvent evaporation. The offset distance between the needles and substrate is not reported. However, this distance appears to be sufficiently small so that the droplets immediately contact the substrate as they are being formed; thus, flight path concerns are irrelevant in this setting. According to the researchers, their results showed that, in the absence of gravity, the surface energy effects would dominate the deposition of the colloids. Furthermore, the droplet dynamics could be manipulated by adjusting the wettability of the needles and the substrate. Lastly, they observed that the more substantial role of surface tension in μg minimized the "coffee ring" pattern, enabling more uniform structures to be printed if coupled with sufficiently fast evaporation.

4.3 Powder Bed Fusion Processes. PBF processes employ a high thermal energy source to selectively fuse regions of a powder bed [179, p. 42]. Each built layer consists of first spreading the powder material, typically with a roller or blade, followed by selectively melting and fusing regions of the powder bed, typically using a laser or electron beam [180,181]. PBF is the most mature metal AM process [66,182], capable of producing fully dense parts with good mechanical properties and high resolution.

Powder-based systems provide several challenges for reduced-gravity environments, including large system footprint compared to build volume, high power requirements, safety hazards due to the use of lasers or electron beams, toxicity and combustibility of metallic powders, and most challenging of all, the difficulty of controlling the movement of the powders in μg, both during the printing process and during the post-processing steps that follow [183]. Furthermore, although recycling the unused powder is possible, provided grain size and powder flowability are monitored [184–187], exchanging material feedstock is a laborious process that may cause powder cross-contamination [188,189]. Methods to facilitate post-processing have been explored [190], but some machining capabilities are generally required. However, PBF has been successfully demonstrated in μg conditions recently. Furthermore, the potential of laser PBF to process lunar regolith simulant was shown by Caprio et al. [191], and other researchers [192,193] are

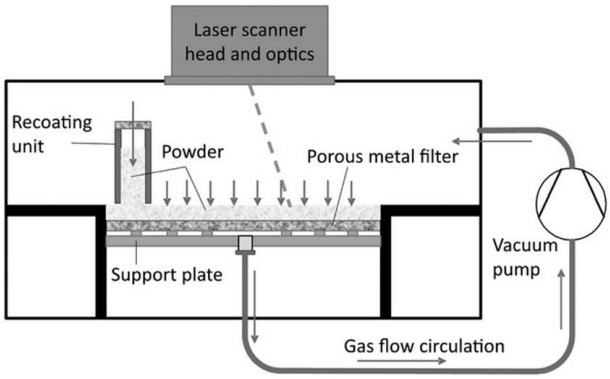

Fig. 2 Schematic of PBF prototype with the flow-assisted method [195]

evaluating the use of the Einstein-Elevator drop tower to test PBF under Lunar and μg.

4.3.1 Parabolic Flight Campaigns—316L Stainless Steel. In 2019, Zocca et al. [194] processed stainless steel type 316L (SS316L) powder in a μg environment via laser PBF. The researchers used a custom PBF system (Fig. 2) that implements their patented "gas flow-assisted powder deposition" method [195] as a novel approach to handling powder feedstock in the absence of gravity. The method uses a porous substrate and a suction pump to create a pressure difference between the top and bottom of the powder bed, thus stabilizing the powder.

The SS316L powder (density = 7.89 g/cm^3) had an apparent packing density of 3.97 g/cm^3 and a particle size distribution D10 of 23.77 μm, D50 of 37.65 μm, and D90 of 62.62 μm. The custom PBF device comprises two units: unit one includes the laser and deposition systems and unit two contains the control system and gas (nitrogen) circulation pump. The PBF device weighed 334 kg and consumed 1200 W of power. The laser system included an IPG 200 W continuous-wave fiber laser emitting at a wavelength of 1070 nm and ScanLab laser optics. The laser was operated at a power output between 100 and 120 W with a spot size on the powder surface of ~48 μm. The base plate (106.5 × 85.5 × 5 mm) is a sinter metal filter made of SS316L with a grade efficiency of 9 μm. The researchers tested three recoaters during the PFCs: (1) a standard roller recoater, (2) a deposition unit that consisted of a box with two parallel edges, and (3) a powder reservoir that is V-shaped at the bottom and ends with a 1 mm slit. The V-shaped recoater employed a piezo actuator to control powder flow and produced the most reproducible layers. In conventional (i.e., terrestrial) PBF, two primary forces, gravitational and interparticle, act on the powder particles. The balance of these two forces controls the flow and packing of the particles in the powder bed. The flow-assisted method introduces drag forces of the same order of magnitude as gravitational forces in μg, thus permitting the stabilization of the powder bed.

The PFCs (Novespace Air Zero G—Airbus A310) included four flights, with 31 parabolas per flight, providing a total of 45 min of μg. Due to the limited time of continuous μg (22 s), powder layer deposition and laser melting took place during phases of different gravity levels. Flights 1–3 were devoted to assessing the feasibility of controlling powder layers in μg via gas flow-assisted powder deposition, with the laser melting occurring in the successive 1g phase. Two wrenches (55 × 12 × ~3 mm) were printed during these three flights using a 0.1 mm layer thickness, 500 mm/s scanning velocity, and a 0.024 mm hatch distance. Flight four was used to study the effects of different gravity conditions in laser melting. Three freestanding walls (1 mm thick) were printed, using the same process parameters, by performing the powder deposition in the 1g phases of the flights and sequentially laser melting one specimen during the μg phase, one specimen during the 1.8 g phase, and the third specimen in 1 g, in the same layer for the three models.

The wrenches were analyzed via optical imaging and X-ray microcomputed tomography, and the walls were analyzed via optical microscopy and electron backscatter diffraction. No defects that could be attributed to μg were found. Optical microscopy demonstrated complete melting within the walls with minimal porosity incidence. Electron backscatter diffraction revealed a microstructure typical for PBF processed SS316L. The researchers stated that microstructure and density should not be affected significantly by the reduced-gravity conditions since, in PBF, the melt pool formation phenomena are driven primarily by surface tension, capillary forces, and inertia; however, due to the limited number of samples that can be printed during PFCs, a comprehensive analysis was not possible. They further stated that PFCs might not be suitable for testing variations in powder bed density, a factor that can affect part quality; thus, PFCs are not suitable for further qualification of gas flow-assisted PBF in μg.

Zocca et al. acknowledged some of the limitations of the gas flow-assisted powder deposition method: Parts with wall thicknesses over 2 mm were not feasible since they would limit the airflow from reaching subsequent layers of powder. Instead of fully dense wrenches, their design adopted hexagonal and single wall infill patterns. The gas flow-assisted powder deposition method is likely subject to other constraints to ensure adequate gas flow, such as limited geometries and support structures. Additionally, a gas flow of 10–20 l/min can only stabilize powder beds up to 80 mm thick. Supplying more than 20 l/min resulted in rough inhomogeneous layers. Powder beds thicker than 80 mm are feasible by increasing the pressure on the top of the building chamber; however, this would likely increase the system footprint further.

4.3.2 Parabolic Flight Campaigns—Polystyrene. D'Angelo et al. [196] developed another method for processing powders independently of g level that places no constraints on feedstock

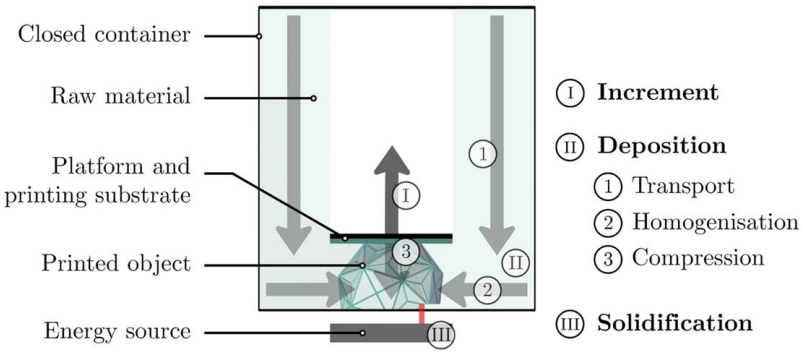

Fig. 3 Schematic of gravity-independent PBF method [197]

flowability. As shown in Fig. 3, the process consists of incrementally raising the printing substrate, on which the part is printed upside down, depositing a layer of powder in three steps, and selectively solidifying the layer. The three-step powder deposition includes three moves: vertical downward transport by screw conveyor, horizontal homogenization by vibration, and compression of the deposited layer. The heat source is supplied through the container's transparent bottom section (i.e., the solidification window). The paper [196] includes a comprehensive description of the multistep deposition process and discrete element method simulations of the powder flow in $1g$ and μg.

PFCs were carried out in Fall 2019 to test a prototype system for use in μg. Three samples (see Table 6) were produced solely during the parabolas' μg phases (lasting ~22 s). The powder deposition occurred during a μg phase, and the solidification step was performed in the subsequent μg phase.

Two types of monodisperse spherical polystyrene powder (mean diameter = 80 μm) are used as feedstock, differing in the surface states, and identified simply as rough surface and smooth surface variants. The prototype system had a printing volume of 65 mm in diameter and 50 mm in height and employed an IR lamp (Quattro IR emitter, power of 500 W) as the heat source. The solidification window is a 5 mm thick fused silica plate. The samples were printed using a 0.5 mm powder layer thickness and a 1.0 mm sintering depth on sintered polystyrene substrates. The substrates were prefabricated by oven sintering (1 h at 200 °C) polystyrene powder on aluminum holders. The IR lamp sinters the entire layer simultaneously; therefore, each sample is obtained by cutting squares (10 × 10 mm) from the center of the substrate. The samples were composed of up to 15 layers if printed in μg and up to 20 layers if printed in $1g$.

The sample listed in Table 6 as "known bad," printed with the rough surface powder in μg, was intentionally solidified with excessive heat to promote partial melting. The sample listed as "known good," printed with the smooth surface powder in $1g$, was oven-sintered (1 h at 200 °C) under a weight of 3 kg in a lab setting. The samples were analyzed via optical imaging and X-ray computed tomography with the resolution set such that the minimum pore size detectable is 15 μm. The average packing fractions are obtained by computing the percent area of material versus voids per slice.

The authors stated that all samples showed homogeneous external surfaces at the macroscale without apparent defects. Furthermore, they noted that sintered densities (Table 6) of good quality samples are expected to be slightly higher than the random close packing (~63% for monosized spheres). The smooth surface samples had higher densities by ~5%, regardless of gravity. Most pores in the smooth surface samples ranged from 15 to 25 μm, with 15 μm pores being twice as likely to appear. In contrast, most pores in the rough surface samples ranged from 15 to 30 μm, with both pore sizes equally likely.

Interestingly, the samples produced in $1g$ showed more substantial pore anisotropy than samples produced in μg. The researchers hypothesized that this is due to the different powder packing before solidification. During the homogenization step, the powder particles form clusters of heterogeneous density. Subsequently, the particles are reordered based on their respective weights resulting in anisotropic packing. Since this reordering is not present in μg, the particles retain the isotropic configuration obtained during the homogenization step. However, the gravitational level does not appear to play a role in the overall porosity distribution of 3D printed samples.

4.3.3 Drop Tower—Regolith Simulant. Reitz et al. [193] processed a Lunar regolith simulant via selective laser melting under the reduced gravity (μg and $0.16g$) and vacuum conditions provided by the Einstein-Elevator and compared them with samples produced under $1g$. The μg phases of the vertical parabolas last 4 s and are preceded by $7.2g$ accelerations, whereas the $0.16g$ phases last 4.4 s and are preceded by accelerations of $6.9g$.

The Lunar regolith simulant (variant TUBS-I) powder had an average grain size of 87 μm and a solid density of 2.84 g/cm^3. The powder is placed inside a metal bowl (70 mm diameter) that can be inserted into the vacuum chamber and fixed with small magnets. The powder is compressed with a homogeneous pressure of 0.64 N/cm^2 before each run to ensure the high acceleration phases do not disturb the feedstock. The experimental payload included a laser housing unit, a vacuum chamber to accommodate the powder feedstock, and a high-speed camera. A 105 W laser with a 976 nm wavelength was set for 3 s per vertical flight. The spherical lens permitted a spot of ~1 mm in diameter to be focused on the powder surface at a working distance of 250 mm. The laser melting process was recorded at 400 frames per second.

The average responses for the various samples printed at each gravity level are tabulated in Table 7. All samples are ellipsoid shaped with a ~3 mm diameter and no apparent visual differences. The samples showed no significant differences in diameter, mass, volume, or porosity. However, the μg samples exhibited the largest scatter for these responses. Eight computerized tomography scans (four $1g$, two $0.16g$, and two μg) permitted analysis of the internal structures, which consist of bubbles of various sizes embedded in a homogeneous green glass-like matrix. All samples were highly porous and included interconnected pores and pores open to the surface. The authors attributed the porosity to the outgassing of volatiles from the regolith simulant, which cannot reach the surface due to the rapid cooling and solidification of the PBF process. Overall, the researchers considered the study a successful proof of concept.

4.4 Directed Energy Deposition Processes. DED is an ASTM/ISO classification for AM technologies "in which focused thermal energy is used to fuse materials by melting as they are being deposited" [56]. Focused heat sources include lasers [197,198], electron beams [199–201], plasma arcs [202,203], and electric arcs [80]. While compatible with polymers and ceramics, DED is mostly associated with metal alloys [204] which can be processed in wire or powder form. Wire feedstocks simplify material handling and increase feedstock efficiency and deposition rates but decrease geometrical capabilities [205]. Regardless of the feedstock form, DED processes commonly require extensive machining operations for parts to achieve acceptable geometries [62, p. 24]; thus, is common for DED to be integrated within CNC machining

Table 6 Sintered densities of polystyrene samples [196]

Sample	Average density (%)
"Known bad"	70.9
SS, μg	69.62
RS, μg	61.69
"Known good"	68.23
SS, $1g$	67.96
RS, $1g$	63.17

Note: SS, smooth surface; RS, rough surface.

Table 7 Laser melting of regolith simulant [193]

Gravity	$1g$	$0.16g$	μg
Samples	4	7	6
Min diameter (mm)	2.74	2.86	2.70
Max diameter (mm)	2.99	3.19	3.24
Roundness	0.126	0.133	0.268
Mass (mg)	17.30	21.29	17.63
Volume (mm^3)	12.21	14.68	13.47
Porosity (%)	49.70	46.77	53.93

systems. The main applications of DED include repairs, feature addition, and production of near-net-shape parts. A recent review of the DED state-of-art is available in Ref. [206].

While DED is used extensively to produce alloy parts for space [207,208], only two μg studies have been found in the literature using aluminum wire feedstocks. Therefore, further insights may be gained by reviewing the effect of μg conditions on welding processes (see review papers [209,210]). DED is being considered for all three ISM scenarios [211,212]. Balla et al. [213] demonstrated using laser DED to process Lunar and Martian regolith simulants. The wire and arc additive manufacturing (WAAM) process is capable of build rates of 9.5 kg/h for steels [214,215] and, by mounting the printhead on a multi-axis robotic arm, can produce parts up to 10 m long [80,216]. WAAM is being implemented by MIS's Vulcan for intravehicular ISM, as discussed in Sec. 5. Lastly, DED technologies that employ electron beams are conducted under vacuum conditions and could be adapted for external ISM.

4.4.1 Parabolic Flight Campaigns—Aluminum 2319. Developed by NASA Langley Research Center (LaRC), electron beam freeform fabrication (EBF^3) uses a focused electron beam to process metal wire under vacuum conditions [217]. LaRC modified a commercial electron beam welder for EBF^3 process development and, collaborating with NASA Johnson Space Center, developed a portable system that could meet PFC requirements [218]. This mobile system included an electron beam welding gun capable of generating a beam with 3–5 kW of power, a much lower value than traditional welding guns (typically ~60 kW), intending to balance radiation risks with a suitable shield, and operated in a high vacuum environment (1×10^{-4} Torr or lower). Other subsystems included a four-axis motion control system that moved the substrate (i.e., build plate), a wire feeder, a vacuum system, and a data acquisition and control system [218,219]. The interior of the portable EBF^3 system showing the major components can be seen in Fig. 4(*a*). EBF^3 is also referred to as electron beam additive manufacturing, Sciaky Inc.'s registered name for the technology [204].

Taminger, the EBF^3 technology Lead, first discussed the potential benefits of this technology in Ref. [217]. Applications included on-orbit construction of large structures and on-demand spare parts fabrication. By 2004, EBF^3 parameters for processing titanium (Ti–6Al–4V) [221] and 2219 aluminum [222] were established. Critical parameters included the beam's voltage and current, the substrate's translation speed, and the wire feeding rate. Surface treatments were also evaluated around this time [223]; milling and wire electrical discharge machining were identified as suitable candidates to achieve 18 root mean square surface finishes with fine-grained equiaxed microstructures at the expense of induced residual stresses. The parts fabricated via EBF^3 demonstrated acceptable machinability using the same CAD data to fabricate the component via EBF^3 [221] and had properties equivalent to those produced via wrought [224]. Gockel et al. discussed progress on EBF^3 process control for processing Ti–6Al–4V in Ref. [225].

In 2007, Hafley et al. conducted PFCs (NASA C-9 Microgravity Research Aircraft) to demonstrate the feasibility of EBF^3 in μg [220]. Additional objectives included evaluating various translation speeds, wire feed rates, and deposition directions for optimal processing in μg, studying the effects of μg on the EBF^3 process, and exploring different directions of wire entry into the melt pool. The PFCs consisted of 11 flights, typically with 40 parabolas per flight and each parabola providing 15–20 s of μg. Material depositions were only conducted during the flights' μg portions. The feedstock, 0.8 mm aluminum (Al2319) wire, was deposited onto 6.35 mm thick aluminum (Al2219) substrates. The initial EBF^3 process parameters (beam power, translation speed, and wire feed rate) were selected based on the researchers' prior work with Al2319 [222]. For comparisons, duplicate samples were prepared in 1g (i.e., on the ground). The analysis included macroscopic photography, manual measurements of the height and width of each deposit using a digital indicator and vernier calipers, respectively, every 12.5 mm along the deposited lengths, and optical microscopy.

The results showed the feasibility of EBF^3 in μg, where the deposited geometry is dominated by surface tension but requires precise control of the distance between the substrate and the wire feeder. As mentioned in Sec. 4.1.1, a similar albeit less strict requirement was identified for FFF. The initial offset distance was programed before the deposition tests and manually adjusted by the operator during the flights. Figures 4(*b*) and 4(*c*) demonstrate deposits made in μg with correct and incorrect (too large) offset distances, respectively. If the distance is too large, molten spheres form at the wire tip, expanding as wire feeding and melting continue. If the distance is too small, the spheres contact the substrate, and capillary forces draw the molten spheres to the deposit. Equivalent offset distances in 1g will produce molten droplets that fall onto the substrate since gravitational forces will exceed surface

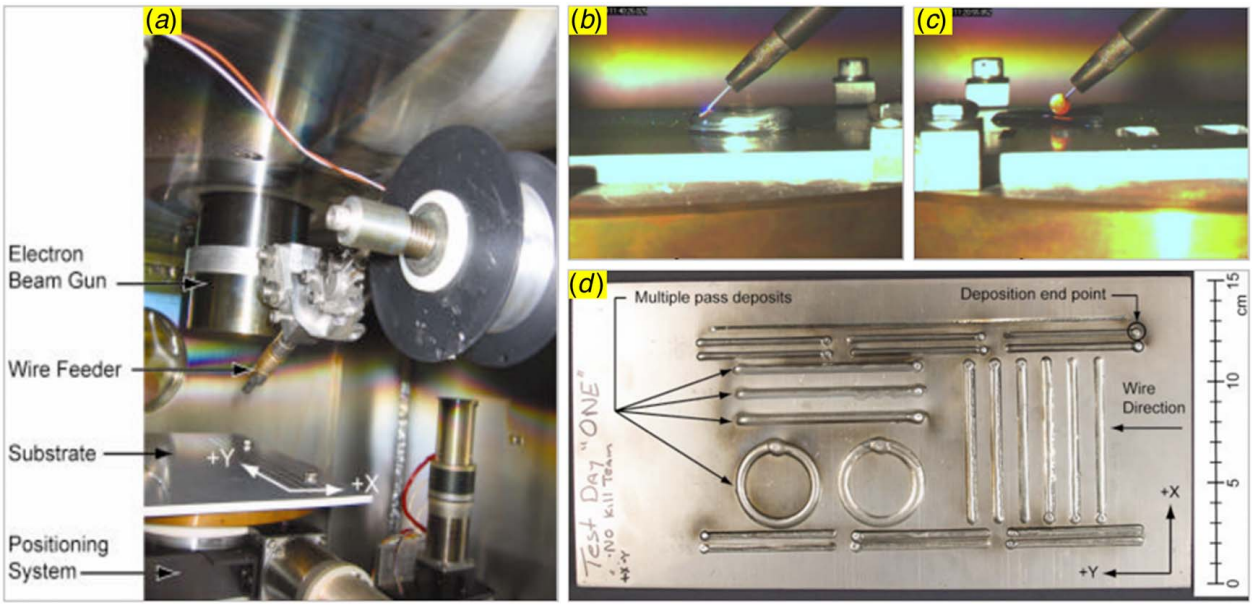

Fig. 4 (*a*) Interior of the portable EBF^3 system. (*b*) Deposit made in μg with the correct distance between the substrate and the wire feeder. (*c*) Deposit made in μg with an incorrect distance between the substrate and the wire feeder. (*d*) EBF^3 deposits conducted in μg to analyze the effects of wire feed rate and direction [220].

tension. Figure 4(*d*) shows the 23 geometries, including four multilayer deposits, printed in μg to explore the effects of translation speeds, wire feed rates, and deposition directions. No visual differences were observed between the geometries fabricated in μg and the equivalent ones manufactured in 1*g*.

Four different directions of wire entry into the melt pool were evaluated to identify differences in deposit height. The height averages (measured in three places on the deposit) and ranges of four deposits printed in μg and 1*g* are illustrated in Fig. 5. The authors noted no clear trend in deposit height as a function of gravity level or wire entry direction.

Optical microscopy analysis (Fig. 6) was based on 45 single-layer deposits produced at each gravity level (i.e., μg and 1*g*) with the same process parameters. The deposits were cross-sectioned, polished, and chemically etched before the analysis. In both cases, the microstructures exhibited columnar grains initiating at the bottom of the melt pool and growing perpendicular to the build plate and are typical of EBF^3 deposits. The microstructures and heat-affected zones are equivalent, and no evidence of porosity was found.

4.4.2 Parabolic Flight Campaigns—Aluminum Alloy. According to Refs. [226,227], researchers from the University of Birmingham tested the effects of μg on a DED process that employed joule heating and "incoherent light" to melt aluminum wire feedstock. The references state that μg experiments via PFCs (ZERO-G Airbus A300) were conducted in 2016, using a DED prototype limited to single-layer extrusion within a 100 mm by 100 mm build area and only consumes 1300 watts of power. The PFCs included three flights, with 31 parabolas per flight, each providing about 22 s of reduced gravity. In addition, the article quotes the researchers stating that the surface tension of the molten metal was used to feed the wire into the substrate and keep it in place and that other methods were developed to keep the material attached to the substrate. Lastly, machining operations would be required for the deposited geometries to reach usable dimensions. Overall, the conclusions appear to agree with those obtained via EBF^3 (Sec. 4.4.1).

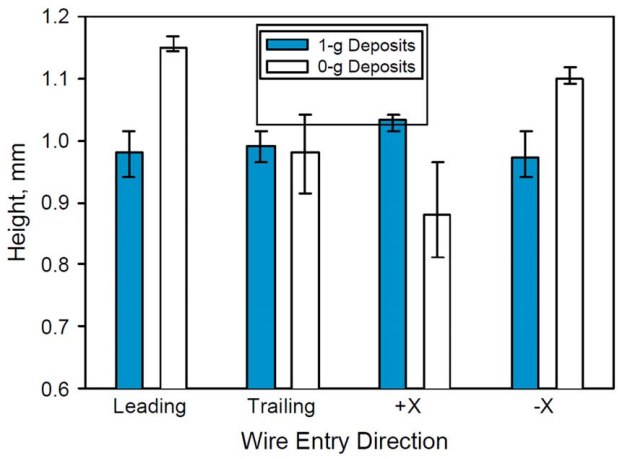

Fig. 5 Comparison of deposit height in 1*g* versus μg (i.e., 0*g*) for four wire entry directions [226]

4.4.3 Directed Energy Deposition μg Simulations. Gu and Li developed computational fluid dynamic transient models accounting for μg and pressure effects in DED processing of 316L stainless steel wire [228]. Their simulation results provided four key insights: (1) irregular deposition tracks would appear in μg due to surface tension dominating the melt pool dynamics; (2) the irregular depositions could be minimized by reducing the wire volume deposited per unit length; (3) material vaporization would more likely occur as pressure was reduced; and (4) lowering laser power or increasing scanning speed could avoid material vaporization. Experimental validation of their model was made by deposition in different orientations under 1*g*.

Xie et al. [229] investigated the evolution and instability of thermocapillary convection in liquid bridges during laser wire (Ti–6Al–4V) DED in reduced gravity. They developed a numerical model to characterize thermocapillary convection and concluded that gravity, or the lack thereof, causes different thermocapillary convection in the metal liquid bridge behavior.

4.5 Vat Photopolymerization Processes. VPP refers to AM processes by which liquid photopolymer, located inside a tank, "is selectively cured by light-activated polymerization" [56]. Two popular VPP technologies include stereolithography and digital light processing (DLP), which employ lasers and projectors, respectively, as the light source. The primary challenge of VPP in μg conditions stems from the limited control of the shape of the liquid layer before photopolymerization. The limited control impacts the recoating process, causing uneven layers and increasing the odds of printing failure. Additionally, while the printing process is largely automated and well-established, labor-intensive pre- and post-processing steps are usually required.

Traditionally limited to resins, VPP can also indirectly process metals and ceramics, as discussed in Sec. 3. Optoform LLC has demonstrated this approach using metal (316L stainless steel, 17–4 *p*H stainless steel, titanium) and ceramic (zircon/silica, alumina, hydroxyapatite) powders [230]. This indirect approach has also been explored to fabricate structures in 1*g* using lunar regolith simulants, as demonstrated in Refs. [231–233].

The website article [234] mentions that MIS's PFCs have included stereolithography experiments. Furthermore, another website article [235] notes that a VPP machine with ceramic resin

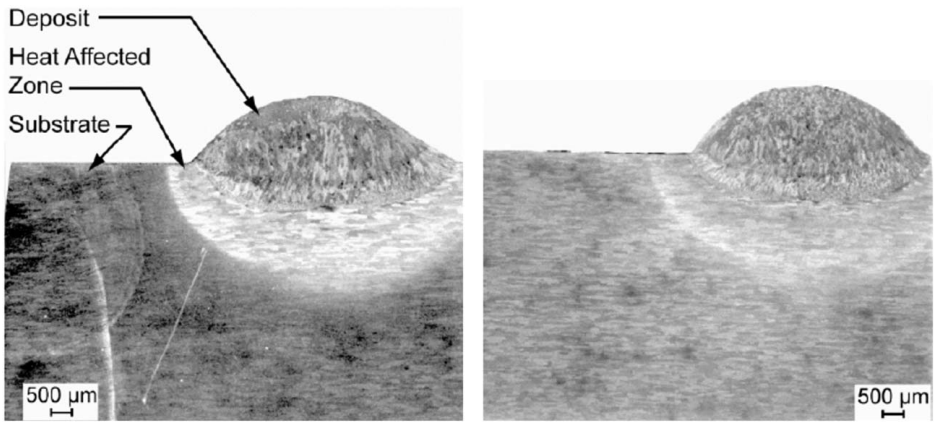

Fig. 6 Microstructure of single-layer deposit produced in μg (left) and 1*g* (right) [226]

processing capabilities, also from MIS, was installed aboard the ISS in December 2020. Unfortunately, no details on these studies were found in the literature.

4.5.1 Parabolic Flight Campaigns—Alumina Resin. Dou et al. [236] demonstrated the feasibility of DLP in μg conditions via PFCs (Novespace Airbus A310 ZERO-G) to process an alumina resin paste. The researchers' approach was to modify the feedstock's rheological properties rather than modify the DLP printing process. The PFCs were conducted in June 2018, according to Ref. [231], and included 16 flights, each providing up to 22 s of reduced gravity.

The researchers [236] tested two ceramic pastes, differing in the thickening agent. The pastes started as ceramic slurries composed of 50 vol% alumina in UV curable resin (triethylene glycol dimethacrylate with photoinitiator 2,4,6-trimethylbenzoyl diphenylphosphine oxide). Then, 5 wt% deionized water and 0.5 wt% thickening agent (hydroxyethyl cellulose or carbomer 940) were added to transform the slurries into pseudoplastic pastes. Pseudoplastic pastes refer to a class of non-Newtonian fluids that show a decrease in viscosity with an increasing rate of shear and demonstrate a solid-like behavior if their applied stress is lower than their yield stress [237].

Dou et al. [236] mentioned that the DLP printer used a light source with a wavelength of 405 nm and a resolution of 50 μm per pixel. An 80 μm layer thickness was selected for the μg tests. However, the exposure time and intensity adjustments to photopolymerize the ceramic paste or additional details on the DLP printer were not reported. After the PFCs, seven as-printed "green" samples were debinded at 600 °C and sintered at 1500 °C in a furnace under an air atmosphere. It is important to note that the DLP printing occurred continuously throughout the flights. The researchers timed the μg phases to identify the layers produced in μg, but any potential impact the hypergravity regimens had on the manufacturing process is difficult to quantify.

The researchers [236] employed X-ray computed tomography with a 5 μm scanning resolution to analyze the internal porosity of the sintered samples layer by layer and determined that the samples printed during the PFCs had an average porosity of 0.63%. However, the researchers point out that the actual porosity may be higher since pores smaller than 5 μm (the scanning resolution) were not included. Additionally, some layers produced in μg were up to 4.41% porous, which the researchers attributed to momentarily uneven recoating. In contrast, based on the Archimedes density measurement method, control samples printed on the ground possessed an average porosity of $0.86 \pm 0.18\%$. The researchers did not identify any relationship between g-level and porosity. They attributed this to the relatively high yield stress of the ceramic pastes, for which the influence of g-level is negligible.

4.6 Binder Jetting Processes. BJT is an ASTM/ISO classification for AM technologies "in which a liquid bonding agent is selectively deposited to join powder materials" [56]. BJT received some attention as a potential planetary ISM technique, as demonstrated by the D-Shape technology [238–240] to build large structures; however, to our knowledge, BJT remains untested in reduced-gravity conditions.

BJT shares process similarities with MJT (Sec. 4.2) and PBF (Sec. 4.3). The deposition of the liquid bonding agent (i.e., the binder) is performed using inkjet printheads identical to those employed by MJT technologies. BJT uses powder recoating methods similar to PBF [61, p. 237]. Therefore, although no BJT studies in μg were found in the literature, the process is technically feasible.

4.7 Sheet Lamination Processes. SHL includes AM technologies "in which sheets of material are bonded to form a part" [56]. Unfortunately, no reduced-gravity SHL studies were found in the literature. However, ultrasonic additive manufacturing (UAM), an SHL variant for processing metals, has been considered for ISM (see Secs. 5.4.1 and 5.4.6). UAM, also known as ultrasonic consolidation, is a hybrid process that combines the solid-state joining of thin (100–150 μm) metal foils and CNC milling to produce metal parts. Solid-state welding is achieved via a rotating sonotrode; thus, thermal stresses or deformations are not encountered [61, p. 263]. UAM is a less established metal AM process than PBF and DED; however, the process is technically feasible for μg experiments.

5 In-Space Manufacturing Technologies Under Development

AM is now predominant within ISM, but additional capabilities are needed for ISM to evolve beyond simple polymeric shapes. For instance, post-processing capabilities (e.g., machining and heat treatments) are necessary for the ISAM of metal parts. Furthermore, in addition to the physical process similarities between welding and metal AM, in-space welding could permit the joining of components limited in size due to AM building volume constraints. Lastly, μg casting could provide another venue for ISM of metals, possibly as a hybrid process (Sec. 5.4.3). For these reasons, traditional manufacturing methods in μg are briefly presented in Secs. 5.1–5.3. Furthermore, hybrid manufacturing (HM) technologies under development are summarized in Sec. 5.4. Lastly, the use of ISAM for life support systems and electronics repair is covered in Secs. 5.5 and 5.6, respectively.

5.1 Welding. As discussed in Ref. [85], several of the physical processes in melt-based AM variants (i.e., DED and PBF) are nearly identical to those in welding; therefore, we refer the reader to two recently published in-space welding papers [209,210] for additional insights. Naden and Prater [209] review the history of in-space welding and describe the adaptation of various welding technologies to be suitable for repair joining operations in space. Liu et al. [210] focus on electron beam welding which is highly relevant to the study discussed in Sec. 4.4.1.

5.2 Casting. Most of the μg research related to casting occurred before 2000 and provided some insights into how solidification in μg differs from that in $1g$, resulting in different microstructures. Summaries of these studies can be found in Refs. [27,241]. Recent μg casting studies are only discussed on websites or are briefly mentioned along with other space-related publications with few details provided. The website article [234] mentions that MIS's PFC included casting experiments, but only an MIS casting patent [242] is available in the literature. The patent describes a method where molten metal is cast into a 3D printed mold to form metal objects. Furthermore, Ref. [243] reported that in June 2018, CAS researchers conducted reduced-gravity metal casting experiments via PFCs, producing eight metal samples. The casting molds were fabricated in $1g$ before the PFCs using the VPP method discussed in Sec. 4.5.1.

5.3 Machining. In 2003, Vincent [244] studied the effect of μg on machining and the feasibility of operating a CNC mill in reduced-gravity environments. PFCs (NASA's KC-135 research aircraft) testing included two separate flights, with 42 parabolas per flight, each with 17–22 s of μg periods. Experimental hardware included a 15 kg Sherline 5100 mill retrofitted with a FlashCut CNC kit and a laptop running FLASHCUT CNC software to control the milling operations. The mill was placed inside a sealed, shatterproof enclosure, connected to a filter and blower assembly that allowed chip collection and air recycling. Milling operations took place during both the microgravitational and $2g$ phases. First flight cuts were made in Aluminum 6061, while more complex operations were done in machinable wax on the second flight. Vincent considers the machining in μg and the chip removal and

collection system to have been successfully demonstrated, and he concluded that the quality of surface cuts is gravity-independent.

5.4 Hybrid Manufacturing Systems. There are several definitions applicable to HM systems (i.e., fabrication machines that combine at least two manufacturing processes), including additive plus subtractive manufacturing, forming plus subtractive manufacturing, two distinct additive manufacturing technologies, and other combinations [245–247]. For the purposes of this paper, the two or more manufacturing processes should occur within the same machine.

The HM projects discussed in this section are the result of NASA SBIR awards and NASA's Multimaterial Fabrication Laboratory (FabLab) initiative [248]. HM projects funded by SBIR awards include the Metal Advanced Manufacturing Bot-Assisted Assembly (MAMBA) process from TUI, Techshot Inc.'s Sintered Metal Printing with Laser Exposure (SIMPLE) technology, and the Vulcan HM system from MIS. The FabLab initiative is being implemented in three phases, starting in May 2017 with NASA's public call seeking partnership proposals for a multimaterial, multiprocess fabrication laboratory to operate aboard the ISS in the 2024 timeframe [249]. Reference [250] highlights that FabLab permits any manufacturing process compatible with μg and the ISS operational constraints. Specifically, FabLab must be teleoperable to reduce dependence on astronaut time, offer a minimum build envelope of six by six-by-six inches, and accommodate ISS EXPRESS Rack constraints, which include a peak power consumption of 2000 W, a weight of 576 lbs, and a volume of 16 cubic feet [167]. Phase A lasted 18 months and focused on developing a ground-based prototype system with inspection capabilities and materials characterization; three companies were selected: Techshot Inc., TUI, and Interlog Corporation [251].

5.4.1 UltraTech Machinery Inc.—Ultrasonic Additive Manufacturing. In 2017, UltraTech Machinery Inc. and subcontractor Fabrisonic LLC received an SBIR phase I award to adapt UAM to manufacture aerospace-grade aluminum parts for ISM while meeting the ISS constraints previously listed [167]. UAM, also known as ultrasonic consolidation, is an HM process that employs ultrasonic welding (combination of ultrasonic energy and compression) to bond thin metal foils to produce near-net shapes, followed by milling to achieve the required dimensions and surface finish [252,253]. UAM's advantages include capabilities to create single and multi-metallic parts in a solid-state manner [254,255], relatively low power requirements [256], and its potential for embedding electronics in the produced structure. As a solid-state welding process, the low temperature causes minimal residual stresses, prevents microstructural changes, and enables the embedding of delicate electronics, wiring, and polymers [257–259].

UltraTech Machinery Inc. phase I focused on designing a 30 kHz sonotrode (a tool that creates ultrasonic energy via vibrations) and demonstrating aluminum alloy (6061-T6 and 7075-T6) welds. Phase I efforts also included designing a motion system for CNC milling to be incorporated in a phase II system and assessing chip debris produced during machining operations. Phase II efforts, awarded in 2018, focused on the CNC milling head incorporation into the UAM system and the assessment of UAM's feasibility for use aboard the ISS [260,261].

5.4.2 Techshot Inc.—SIMPLE. Techshot Inc.'s SIMPLE project was awarded an SBIR phase I award in June 2016, with the goal of enabling metal processing capabilities in space. The device processes metal filament by first using induction to heat the filament to its Curie temperature, and upon its deposition, it is fused to the build plate or previous layer by exposure to a laser. In contrast to the induction heating used by FFF extruders, SIMPLE's induction coil heats the wire directly [262,263]. Phase II concluded in January 2020, with SIMPLE reaching an estimated TRL-6 [264].

5.4.3 Tethers Unlimited Inc—MAMBA. In June 2017, TUI received an SBIR phase I award to develop the MAMBA hybrid process, which seeks to combine forming and milling, along with robotic capabilities, to enable the manufacturing of metals in space [265]. MAMBA builds on TUI's Refabricator work, discussed in Sec. 4.1.8, to shape metal ingots from virgin or scrap metal, which subsequently undergoes CNC machining [266]. Phase II concluded in December 2020, with MAMBA reaching an estimated TRL-5 [267].

5.4.4 Made In Space Inc—Vulcan. Funded in June 2017 through an SBIR phase I award, MIS's Vulcan HM system incorporates easily interchangeable FFF and WAAM manufacturing heads for processing polymers and aluminum wire. As in typical wire DED operations, the deposition process requires an inert shield gas and subsequent CNC machining. Vulcan integrates additive and subtractive manufacturing within one machine, reducing footprint requirements [268]. Vulcan also integrates an iris clamp and robotic gripper subsystem to automate fixturing and machining operations and an environmental control unit to handle fumes and chip debris formation [131]. Vulcan reached an estimated TRL-6 in February 2021 (i.e., the end of the SBIR phase II period) [269], and along with Techshot Inc.'s FabLab (discussed in Sec. 5.4.7), is one of two processes in development as future ISS payload and thus must meet the EXPRESS Rack constraints listed previously [131].

5.4.5 Tethers Unlimited Inc—FabLab. TUI's FabLab efforts focused on autonomous processing combined with verification and validation services for μg-enabled multimaterial manufacturing. Specifically, the development of a robotic arm for the movement of printed components between subsystems and a structured light scanning subsystem compares the dimensions of the printed part against the CAD model to verify dimensional tolerances [249]. However, Edmunson et al. [168] reported that an unsuccessful preliminary design review took place in August 2019, lacking design and analysis details.

5.4.6 Interlog Corporation—FabLab. Interlog Corporation's FabLab aimed to develop a μg-enabled multimaterial AM technology based on a proprietary wire-fed UAM technique that combines a focused-energy bonding mechanism and a machining subsystem [167]. Unfortunately, the process proved unsuccessful for aluminum alloys resulting in the project's conclusion in December 2019 [168].

5.4.7 Techshot Inc.—FabLab. Techshot Inc.'s FabLab aims to enable metal ISM capabilities by integrating BMD (i.e., metal FFF), furnace-based thermal treatments, machining, and in situ inspection subsystems [160,168]. Technology demonstrations focused on processing Ti–6Al–4V filament (59 vol% metal powder) developed by the University of Louisville, and sintered densities up to 97.2% are reported [131,270]. The FabLab system and MIS's Vulcan (Sec. 5.4.4) are the two metal AM technologies under current consideration for ISS demonstrations in 2025 [131].

Extensive information on the BMD of Ti–6Al–4V can be found in the doctorate dissertation [270]. We note that the work conducted by the University of Louisville [270] employed a two-step debinding procedure: solvent-based debinding and thermal debinding in a furnace. However, the FabLab system only uses thermal debinding in a furnace, which is not as effective at removing large quantities of binder; thus, possible geometries (e.g., thick solid parts) and mechanical properties may be limited.

Lastly, terrestrial and μg-based BMD material modeling simulations were performed by Luchinsky et al. [271] to analyze the nonlinear shrinkage during sintering, a concern shared by all indirect metal AM technologies. The researchers combined multi-scale physics-based and data-driven approaches for shrinkage prediction, providing the required compensation for the printed part.

5.5 ISAM for Life Support Systems. Prolonged exposure to the space environment (e.g., μg and increased radiation) has been associated with the deterioration of muscles and bone tissue [272] and weakened immune systems [273,274]. These observations are based on the typical rotation of ISS astronauts every six months; however, deep space missions to locations such as Mars are estimated to take longer. In-space bioprinting could facilitate such long-term studies; for instance, Gelinsky [38] mentions that compared with conventional cell cultures, bioprinted 3D tissue models are more representative of the human body and could be used to study the long-term effects of space radiation and μg. Furthermore, in-space bioprinting could offer treatments in case of space crew injuries.

Bioprinting is differentiated among AM processes by its feedstock (e.g., cell-laden bioinks and biomaterials [275]) to create 3D functional living tissues or artificial organs [276]. Like most AM processes, bioprinting requires multiple steps: preprocessing, where the digital blueprint is prepared, printing using different techniques, and post-processing, where the bioprinted artifact undergoes remodeling and maturation in a bioreactor. Comprehensive bioprinting reviews are provided in Refs. [277,278].

In addition to the 3D BioFabrication Facility discussed in Sec. 4.1.9, a second bioprinter has been tested in continuous μg conditions. The 3D Bioprinting Solutions Organaut, created by the company 3D Bioprinting Solutions in collaboration with Roscosmos, reached the ISS in December 2018. It utilizes magnetic particles to develop clusters of cells and has demonstrated the feasibility of scaffold-free formative biofabrication [279].

5.6 ISAM for Electronics Repair. Prater et al. [154] indicated that many past ISS failures have been electronics-based. Therefore, NASA considers an in-space electronics manufacturing capability critical for deep space missions. The interested reader can refer to Refs. [280] for a report on flexible printed electronics for NASA missions and to Ref. [281] for a discussion on nanosensors and nanoelectronics for space exploration needs. Other emerging applications include the fabrication of sensors for ISS air quality monitoring [282–284], sensors to detect cracks on solid structures [285], and printable power generators [286,287].

Several projects, including SBIR awards, have focused on adapting aerosol DW for electronics ISM. Aerosol DW processes, such as Optomec Inc.'s aerosol jet printing, make deposits from inks (i.e., colloidal suspensions) suspended as an aerosol via atomization [288]. Researchers from MSFC investigated thermal atomization for the aerosol mist generation of inks for printing electronics in space [289]. Optomec Inc.'s adaptive laser sintering system SBIR project focused on enhancing aerosol jet printing capabilities by reducing thermal damage to polymer substrates during the sintering of metal inks [290,291]. Plasma jet printing, an aerosol DW variant with an estimated TRL-5, processes a feedstock that is aerosolized and focused using an electromagnetic field and plasma, providing enhanced printing directionality [292]. Electronics manufacturing has also been demonstrated by applying other AM technologies [107,293–296].

Table 8 Publications breakdown by material

Material	Publications
ABS	[37,132,136,146,157]
Aluminum alloys	[220,222,226–269]
PLA	[137,149,150]
Polystyrene	[178,196]
Alumina resin	[235,236]
Aqueous glycerol	[176,177]
Regolith simulant	[191,193]
Stainless steel 316L	[194,228]
Ti–6Al–4V	[131,221,229,270]
ULTEM 9085	[166,167,297]

6 Categorization of Research Efforts

A classification of AM researched in reduced-gravity conditions by type of material processed is presented in Table 8.

A second classification, by manufacturing process type, is presented in Table 9. Some of the MEX systems tested were commercial, with little or no modification needed before the study. In contrast, for metal AM (i.e., DED and PBF), all systems tested were custom-made for the PFCs and would require significant improvements to be compatible with platforms such as the ISS. Ceramic AM is hardly discussed in intravehicular ISM publications, using VPP to process ceramic resins that would require debinding and sintering.

7 Insight and Future Research

Key obstacles contributing to slowing down advancements in ISAM include quality, cost, and limited access to research platforms. The quality of AM parts is typically quantified via metrics, including the extent of defects in a part (e.g., porosity, warping, and delamination), mechanical properties, geometric accuracy, and repeatability. The lack of repeatability (or high degrees of variability) has been identified among the most pressing obstacles hindering wider adoption of AM in general [64] for terrestrial or ground-based (i.e., $1g$) applications. It is attributed to our lack of understanding of the complex physics associated with AM processes, in addition to other factors such as machine-to-machine variability, raw feedstock variability, design considerations (e.g., build orientation), and the manufacturing environment (e.g., the layout of parts on the building substrate or circulation of the inert atmosphere inside the chamber) among many others [298]. While high degrees of variability in AM parts complicate concluding how the quality of parts produced in μg compares to their ground-based counterparts, the AM studies reviewed (Sec. 4) generally indicate similarity in microstructures of AM parts (which drive mechanical properties) produced in μg as in $1g$.

Limited access to μg research platforms (Table 1) has also represented an obstacle. Aircraft PFCs remain the most common platform for ISAM research, as they can accommodate the size of the equipment and permit investigator intervention if needed. However, PFCs introduce hypergravity phases and only offer 15–25 s of continuous μg, which is unsuitable for conducting substantiated statistical analysis since only a few samples can be produced.

Polymer ISAM via FFF has reached considerable maturity (TRL-9, according to Ref. [161]). Three FFF machines were tested aboard the ISS, including the AMF, which offers commercial printing services to print parts that can be down massed to Earth for analysis [138]. However, some capabilities available for Earth-based FFF machines have not been demonstrated in space. For example, support structures are not permitted for the AMF [138], and no geometry which would require support structures and subsequent post-processing has been identified in the literature. While this constraint may be placed only to minimize time demands on ISS astronauts, no evidence of a procedure to remove support structures or safely handle the resulting waste has been reported. With recycling initiatives demonstrated by TUI's ReFabricator (Sec. 4.1.8) and future ISS demonstrations planning to incorporate

Table 9 Publications breakdown by process

Process	Publications
MEX	[37,131,132,134,136,137,146,150,157,158]
DED	[217–221,223,224,226–229]
PBF	[191–194,196]
VPP	[231,234–236]
MJT	[175–178]

machining capabilities, future work could combine these efforts to expand FFF applications. Furthermore, the capabilities of currently available FFF devices aboard the ISS could also be extended to indirectly process metals and ceramics, as discussed in Sec. 3.1, if an ISM furnace was to be designed and certified for necessary post-processing. Furnace systems have been tested aboard the ISS [299], but handling the polymer binder waste in μg remains challenging.

Metal ISAM has only been demonstrated via three PFCs: NASA LaRC focused on electron beam DED with an aluminum wire feedstock; a collaboration between the University of Birmingham and the European Space Agency also showed a DED process with aluminum wire but adopted Joule heating and incoherent light to melt the wire; and more recently, researchers from the Federal Institute for Materials Research and Testing, Novespace, and German Aerospace Center showed the feasibility of laser-based PBF to process 316L stainless steel. PFCs are vital precursors for validating an ISM process but do not generate enough data to enable statistical analysis. Furthermore, these studies do not address how the required post-processing would be achieved under intravehicular space conditions. The three processes tested would also require machining capabilities to separate the built part from the building plate. It is important to point out that sample cleaning (i.e., de-powdering) and separation from the base plate took place after the PFC. Separation of metal parts from the base plate typically requires machining operations such as bandsaw cutting or wire electrical discharge machining, which produce swarf debris and could pose a danger for intravehicular operations. In addition, larger artifacts with more elaborate geometries would also require support structures and sequential removal, further increasing the need for dedicated μg machining and other post-processing equipment. Elementary machining operations have been successfully demonstrated in μg conditions (see Sec. 5.3). However, hybrid manufacturing, where additive and subtractive operations occur within a unified system, or sequential machining operations after AM, remain untested in μg.

As discussed in Sec. 5, NASA MSFC has narrowed down two candidate processes for metal ISAM aboard the ISS by 2025: MIS's Vulcan, an HM system that combines WAAM and CNC machining to process aluminum; and Techshot Inc.'s Fablab, which uses FFF to process titanium-polymer filaments, thus requiring debinding and sintering. The Vulcan system also includes machining capabilities and a robotic gripper to automate the process further. The FabLab is only supposed to require crew interaction during installation, to move a part between subsystems, and to change feedstock. Integrating the various subsystems into a single device for either system represents a significant technical challenge further complicated by the requirement to accommodate ISS EXPRESS Rack constraints. Vulcan benefits from insights from welding studies in μg conditions (Sec. 5.1). Still, as a WAAM process, it will likely have limited geometrical capabilities and produce significant waste due to the extensive machining required. Thermal stresses associated with WAAM, potentially magnified in μg, will also need to be addressed. FabLab benefits from μg FFF insights and the "office-friendly" nature of this indirect metal process, which could include dual FFF extruders to obtain hand-removable supports. One challenge stems from the non-uniform shrinkage associated with the sintering stage. Furthermore, the thermal debinding will limit achievable thicknesses, compromising the metal parts' maximum functionality and creating the need to handle and dispose of toxic binder substances.

8 Summary

Over the past 20 years, AM has received increasing attention for ISM due to its geometric freedom and reduced material waste, among other benefits. The effect of reduced-gravity conditions on MEX processing of polymers has been investigated extensively since 1999, with three MEX machines tested aboard the ISS in the last decade. As a result, polymer-based MEX appears to be gravity-independent. However, AM of metals and ceramics has only been tested aboard short μg duration platforms that are insufficient for statistical analysis due to the limited data. In addition, safety considerations and the need for auxiliary equipment and manual labor to perform post-processing tasks further complicate the adaptation of metal AM systems for orbital spacecraft.

This paper conducted a critical literature review of ISAM and its related technologies and summarized available studies from academia and industry in this area. In addition to providing a detailed discussion of the ISAM state-of-art and identifying knowledge gaps, we categorized ISM research efforts according to the manufacturing process and type of material involved.

Acknowledgment

The authors are grateful for NASA's support under Grant No. 80NSSC19K1052. Any opinions, findings, and conclusions or recommendations expressed in this material are those of the authors and do not necessarily reflect the views of NASA.

Conflict of Interest

There are no conflicts of interest.

Data Availability Statement

The datasets generated and supporting the findings of this article are obtainable from the corresponding author upon reasonable request.

References

[1] Owens, A., and De Weck, O., 2016, "Systems Analysis of In-Space Manufacturing Applications for the International Space Station and the Evolvable Mars Campaign," AIAA SPACE 2016, Long Beach, CA, Sept. 13–16, p. 5394.

[2] Vickers, J., 2020, "NASA's Additive Manufacturing Technology-Driving Exploration," Lunar Excavation, Manufacturing, and Construction Challenge-Ideation Workshop, Document ID 20200001736.

[3] Lotz, C., Frobose, T., Wanner, A., Overmeyer, L., and Ertmer, W., 2017, "Einstein-Elevator: A New Facility for Research From μg to $5g$," Gravitational Space Res., **5**(2), pp. 11–27.

[4] Lotz, C., Wessarges, Y., Hermsdorf, J., Ertmer, W., and Overmeyer, L., 2018, "Novel Active Driven Drop Tower Facility for Microgravity Experiments Investigating Production Technologies on the Example of Substrate-Free Additive Manufacturing," Adv. Space Res., **61**(8), pp. 1967–1974.

[5] Rosenthal, B. N., Glasgow, T. K., Black, R. E., and Elleman, D. D., 1987, "Research Opportunities in Microgravity Science and Applications During Shuttle Hiatus," https://ntrs.nasa.gov/citations/19870007484

[6] Meseguer, J., Sanz-Andrés, A., Pérez-Grande, I., Pindado, S., Franchini, S., and Alonso, G., 2014, "Surface Tension and Microgravity," Eur. J. Phys., **35**(5), p. 055010.

[7] Pletser, V., 2020, *Preparation of Space Experiments*, BoD–Books on Demand.

[8] Beysens, D. A., and van Loon, J. J., 2015, *Generation and Applications of Extra-Terrestrial Environments on Earth*, River Publishers, Aalborg.

[9] Matthews, K. R., Motiwala, S. A., Edberg, D. L., and Garcia-Llama, E., 2012, "Flight Mechanics Experiment Onboard NASA'S Zero Gravity Aircraft," J. Technol. Sci. Educ., **2**(1), pp. 4–12.

[10] Sabbatini, M., 2014, "ESA User Guide to Low Gravity Platforms," Directorate of Human Spaceflight and Operations, Noordwijk, The Netherlands.

[11] Ferranti, F., Del Bianco, M., and Pacelli, C., 2020, "Advantages and Limitations of Current Microgravity Platforms for Space Biology Research," Appl. Sci., **11**(1), p. 68.

[12] Duan, E., and Long, M., eds., 2019, *Life Science in Space: Experiments on Board the SJ-10 Recoverable Satellite*, Springer, New York.

[13] Soares, C., Mikatarian, R., and Schmidl, D., 2005, "Natural and Induced Space Environments Effects on the International Space Station," 56th International Astronautical Congress.

[14] Prater, T., 2020, "In-Space Manufacturing (ISM): Make It, Don't Take It!," https://ntrs.nasa.gov/api/citations/20200001731/downloads/20200001731.pdf, Accessed July 22, 2021.

[15] Newman, D. J., 2007, "Life in Extreme Environments: How Will Humans Perform on Mars?," Gravitational Space Res., **13**(2), pp. 35–47.

[16] Thirsk, R., Kuipers, A., Mukai, C., and Williams, D., 2009, "The Space-Flight Environment: The International Space Station and Beyond," CMAJ, **180**(12), pp. 1216–1220.

[17] Dorsey, J., Doggett, W., McGlothin, G., Alexandrov, N., Allen, B. D., Chandarana, M., Cooper, J., Vie, L. L., Neilan, J., Puig Navarro, J., and

Waltz, W., 2021, "State of the Profession: NASA Langley Research Center Capabilities/Technologies for Autonomous In-Space Assembly and Modular Persistent Assets," Bull. Am. Astron. Soc., **53**(4), p. 389.
[18] Moraguez, M. T., 2018, "Technology Development Targets for Commercial In-Space Manufacturing," Ph.D. thesis, Massachusetts Institute of Technology, Cambridge, MA.
[19] NASA's Exploration & In-Space Services, OSAM-1 Mission: On-orbit Servicing, Assembly, and Manufacturing 1, https://nexis.gsfc.nasa.gov/OSAM-1.html, Accessed July 10, 2021.
[20] Boyd, I., 2017, "On Orbit Manufacturing and Assembly of Spacecraft," Technical Report, Institute for Defense Analyses.
[21] Piskorz, D., and Jones, K. L., 2018, *On-Orbit Assembly of Space Assets: A Path to Affordable and Adaptable Space Infrastructure*, The Aerospace Corporation, El Segundo.
[22] Clinton, Jr, R., Werkheiser, N., Prater, T., Ledbetter, F., Laughinghouse, T., Adams, C., Clinton, T., Shestople, P., and Lymer, J. D., 2019, AM in Space: ISM and IRMA NASA Initiatives, https://ntrs.nasa.gov/citations/20190005001, Accessed July 10, 2021.
[23] Lymer, J., Doggett, W. R., Dorsey, J., Bowman, L., Tadros, A., Hollenstein, B., King, B., Emerick, K., Hanson, M., and Boccio, J. D., 2016, "Commercial Application of In-Space Assembly," AIAA SPACE 2016, Long Beach, CA, Sept. 13–16, p. 5236.
[24] Sacksteder, K., and Sanders, G., 2007, "In-Situ Resource Utilization for Lunar and Mars Exploration," 45th AIAA Aerospace Sciences Meeting and Exhibit, Reno, NV, Jan. 8–11, p. 345.
[25] Rice, E., and Gustafson, R., 2000, "Review of Current Indigenous Space Resource Utilization (ISRU) Research and Development," 38th Aerospace Sciences Meeting and Exhibit, Reno, NV, Jan. 10–13, p. 1057.
[26] Schollharnmer, F., 1967, "Hand-Held Electron Beam Gun for In-Space Welding," 4th Space Congress Proceedings vol. 5, Cocoa Beach, FL, Apr. 3.
[27] National Research Council, 2000, *Microgravity Research in Support of Technologies for the Human Exploration and Development of Space and Planetary Bodies*, National Academies Press, Washington, DC.
[28] Wilson, M. L., MacConochie, I. O., and Johnson, G. S., 1987, "Potential for On-Orbit Manufacture of Large Space Structures Using the Pultrusion Process," NASA Technical Memorandum, Hampton, VA, Jan. 1.
[29] Watson, K., Petersen, D., and Crockett, R., 1999, "Application of Solid Freeform Fabrication Technology to NASA Exploration Missions," Proceedings From the SFF Symposium, Austin, TX, Aug. 9–11, pp. 857–864.
[30] Wohlers, T., and Gornet, T., 2014, "History of Additive Manufacturing," Wohlers Rep., **24**, p. 118.
[31] Skomorohov, R., Welch, C., and Hein, A. M., 2016, "In-Orbit Spacecraft Manufacturing: Near-Term Business Cases Individual Project Report," Research Report, International Space University/Initiative for Interstellar Studies.
[32] Clinton, R., Jr., 2016, "NASA's In Space Manufacturing Initiative For Exploration-Why, How, What!: Manufacturing Problem Prevention Program," https://ntrs.nasa.gov/api/citations/20160013275/downloads/20160013275.pdf.
[33] Clinton, R., Prater, T., Werkheiser, N., Morgan, K., and Ledbetter, F. E., 2018, "NASA Additive Manufacturing Initiatives for Deep Space Human Exploration," 69th International Astronautical Congress (IAC), Bremen, Germany, Oct. 1–5.
[34] Ghidini, T., 2013, "An Overview of Current AM Activities at the European Space Agency," 3D Printing & Additive Manufacturing—Industrial Applications Global Summit, London, UK.
[35] Zhang, Y. Y., Jin, Z. J., and Zhang, W., 2020, "Application of 3d Printing in Future Manned Space Exploration," *Materials Science Forum*, Y. Zhao, ed., Vol. 982, Trans Tech Publ., pp. 92–97.
[36] Hurley, B., "3D Printing and Space Exploration: How NASA Will Use Additive Manufacturing," https://www.techbriefs.com/component/content/article/tb/stories/blog/35871.
[37] Bean, Q., Cooper, K., Edmunson, J., Johnston, M., and Werkheiser, M., 2015, "International Space Station (ISS) 3d Printer Performance and Material Characterization Methodology," https://ntrs.nasa.gov/citations/20150016234.
[38] Gelinsky, M., 2020, "Latest Advances of Bioprinting in Space: An Interview With Michael Gelinsky," J. 3D Print. Med., **4**(1), pp. 1–4.
[39] Kading, B., and Straub, J., 2015, "Utilizing In-Situ Resources and 3d Printing Structures for a Manned Mars Mission," Acta Astronaut., **107**, pp. 317–326.
[40] Mankins, J. C., 1995, "Technology Readiness Levels," White Paper, April 6, p. 1995.
[41] National Research Council, 2014, *3D Printing in Space*, National Academies Press, Washington, DC.
[42] Dordlofva, C., Lindwall, A., Törlind, P., 2016, "Opportunities and Challenges for Additive Manufacturing in Space Applications," DS 85-1: Proceedings of Nord Design 2016, Trondheim, Norway, Aug. 10–12, Vol. 1, pp. 401–410.
[43] Marc Abi-Fadel, M., Al Harbi, M., Chafena, M., Chen, T., Farias, A., Halpina, S., Jiang, Z., et al., 2019, "Leveraging Additive Manufacturing to Enable Deep Space Crewed Missions," 70th International Astronautical Congress (IAC), Washington, DC, Oct. 21–25.
[44] Moraguez, M., and de Weck, O., 2019, "Suitability of Manufacturing Processes for In-Space Manufacturing of Spacecraft Components," 70th International Astronautical Congress (IAC), Washington, DC, Oct. 21–25
[45] Moraguez, M., and de Weck, O., 2020, "Benefits of In-Space Manufacturing Technology Development for Human Spaceflight," 2020 IEEE Aerospace Conference, Big Sky, MT, Mar. 7–14, IEEE, pp. 1–11.
[46] Sacco, E., and Moon, S. K., 2019, "Additive Manufacturing for Space: Status and Promises," Int. J. Adv. Manuf. Technol., **105**(10), pp. 4123–4146.
[47] Shevtsova, V., Lyubimova, T., Saghir, Z., Melnikov, D., Gaponenko, Y., Sechenyh, V., Legros, J. C., and Mialdun, A., 2011, "Ividil: On-Board g-Jitters and Diffusion Controlled Phenomena," J. Phys.: Conf. Ser., **327**, p. 012031.
[48] Thomas, V., Prasad, N., and Reddy, C. A. M., 2000, "Microgravity Research Platforms—A Study," Curr. Sci., **79**(3), pp. 336–340.
[49] Brooks, J., Reavis, J., Medwood, R., Stalcup, T., Meisel, M., Steinberg, E., Arnowitz, L., Stover, C., and Perenboom, J., 2000, "New Opportunities in Science, Materials, and Biological Systems in the Low-Gravity (Magnetic Levitation) Environment," J. Appl. Phys., **87**(9), pp. 6194–6199.
[50] Lemmer, K., 2017, "Propulsion for Cubesats," Acta Astronaut., **134**, pp. 231–243.
[51] Pletser, V., 2020, "Aircraft Parabolic Flights: A Gateway to Orbital Microgravity and Extra-Terrestrial Planetary Gravities," *Preparation of Space Experiments*, V. Pletser, ed., IntechOpen.
[52] Kumar, L. J., and Nair, C. K., 2017, "Current Trends of Additive Manufacturing in the Aerospace Industry," *Advances in 3D Printing & Additive Manufacturing Technologies*, D. Wimpenny, P. L. Pandey, and J. Kumar, eds., Springer, New York, pp. 39–54.
[53] Blakey-Milner, B., Gradl, P., Snedden, G., Brooks, M., Pitot, J., Lopez, E., Leary, M., Berto, F., and du Plessis, A., 2021, "Metal Additive Manufacturing in Aerospace: A Review," Mater. Des., **209**, p. 110008.
[54] Song, Y., Yan, Y., Zhang, R., Xu, D., and Wang, F., 2002, "Manufacture of the Die of an Automobile Deck Part Based on Rapid Prototyping and Rapid Tooling Technology," J. Mater. Process. Technol., **120**(1–3), pp. 237–242.
[55] Kumar, R., Kumar, M., and Chohan, J. S., 2021, "The Role of Additive Manufacturing for Biomedical Applications: A Critical Review," J. Manuf. Process., **64**, pp. 828–850.
[56] ASTM, ISO, 2015, *ASTM52900-15 Standard Terminology for Additive Manufacturing—General Principles—Terminology*, ASTM International, West Conshohocken, PA.
[57] Bin Ishak, I., Fisher, J., and Larochelle, P., 2016, "Robot Arm Platform for Additive Manufacturing Using Multiplane Toolpaths," International Design Engineering Technical Conferences and Computers and Information in Engineering Conference, Charlotte, NC, Aug. 21–24, American Society of Mechanical Engineers, Vol. 50152, p. V05AT07A063.
[58] Padhy, S. K., 1992, "On the Dynamics of Scara Robot," Rob. Auton. Syst., **10**(1), pp. 71–78.
[59] Carp-Ciocardia, D., 2003, "Dynamic Analysis of Clavel's Delta Parallel Robot," 2003 IEEE International Conference on Robotics and Automation, IEEE, Vol. 3, pp. 4116–4121, Cat. No. 03CH37422.
[60] Deshpande, S. P., Kulkarni, S., Shah, S., and Irwin, J., 2019, "Developing an Open Source, Inexpensive, Large-Scale Polar Configuration 3d Printer," Int. J. Eng. Res. Innov., **11**(2), pp. 13–22.
[61] Gibson, I., Rosen, D. W., Stucker, B., and Khorasani, M., 2021, *Additive Manufacturing Technologies*, Vol. 17, Springer, New York.
[62] Yang, L., Hsu, K., Baughman, B., Godfrey, D., Medina, F., Menon, M., and Wiener, S., 2017, *Additive Manufacturing of Metals: The Technology, Materials, Design and Production*, Springer, New York.
[63] Srivastava, M., Rathee, S., Maheshwari, S., and Kundra, T., 2019, *Additive Manufacturing: Fundamentals and Advancements*, CRC Press, Boca Raton, FL.
[64] Tapia, G., and Elwany, A., 2014, "A Review on Process Monitoring and Control in Metal-Based Additive Manufacturing," ASME J. Manuf. Sci. Eng., **136**(6), p. 060801.
[65] Bian, L., Shamsaei, N., and Usher, J. M., 2017, *Laser-Based Additive Manufacturing of Metal Parts: Modeling, Optimization, and Control of Mechanical Properties*, CRC Press, Boca Raton, FL.
[66] Chua, C. K., Wong, C. H., and Yeong, W. Y., 2017, *Standards, Quality Control, and Measurement Sciences in 3D Printing and Additive Manufacturing*, Academic Press, London.
[67] Lim, J. X.-Y., and Pham, Q.-C., 2021, "Automated Post-Processing of 3d-Printed Parts: Artificial Powdering for Deep Classification and Localisation," Virtual Phys. Prototyp., **16**(3), pp. 333–346.
[68] Nelaturi, S., Behandish, M., Mirzendehdel, A. M., and de Kleer, J., 2019, "Automatic Support Removal for Additive Manufacturing Post Processing," Comput. Aided Des., **115**, pp. 135–146.
[69] Becker, P., Eichmann, C., Ronnau, A., and Dillmann, R., 2020, "Automation of Post-Processing in Additive Manufacturing With Industrial Robots," 2020 IEEE 16th International Conference on Automation Science and Engineering (CASE), Hong Kong, China, Aug. 20–21, IEEE, pp. 1578–1583.
[70] Standard, A., 2014, D638 (2014) Standard Test Method for Tensile Properties of Plastics, ASTM International, West Conshohocken, PA.
[71] Specimens, P., 2014, Standard Test Methods for Flexural Properties of Unreinforced and Reinforced Plastics and Electrical Insulating Materials, ASTM International, West Conshohocken, PA.
[72] For Testing, A. S., and Materials, 2015, "Standard Test Method for Compressive Properties of Rigid Plastics," Report D695-15.
[73] Charalampous, P., Kostavelis, I., and Tzovaras, D., 2020, "Non-destructive Quality Control Methods in Additive Manufacturing: A Survey," Rapid Prototyp. J., **26**(4), pp. 777–790.
[74] Ding, D., Shen, C., Pan, Z., Cuiuri, D., Li, H., Larkin, N., and van Duin, S., 2016, "Towards an Automated Robotic Arc-Welding-Based Additive Manufacturing System From CAD to Finished Part," Comput. Aided Des., **73**, pp. 66–75.
[75] Urhal, P., Weightman, A., Diver, C., and Bartolo, P., 2019, "Robot Assisted Additive Manufacturing: A Review," Robot. Comput. Integr. Manuf., **59**, pp. 335–345.

[76] Bhatt, P. M., Malhan, R. K., Shembekar, A. V., Yoon, Y. J., and Gupta, S. K., 2020, "Expanding Capabilities of Additive Manufacturing Through Use of Robotics Technologies: A Survey," Addit. Manuf., **31**, p. 100933.
[77] Wu, C., Dai, C., Fang, G., Liu, Y.-J., and Wang, C. C., 2017, "Robofdm: A Robotic System for Support-Free Fabrication Using FDM," 2017 IEEE International Conference on Robotics and Automation (ICRA), Singapore, May 29–June 3, IEEE, pp. 1175–1180.
[78] Shembekar, A. V., Yoon, Y. J., Kanyuck, A., and Gupta, S. K., 2018, "Trajectory Planning for Conformal 3d Printing Using Non-Planar Layers," International Design Engineering Technical Conferences and Computers and Information in Engineering Conference, Quebec City, Quebec, Canada, Aug. 26–29, American Society of Mechanical Engineers, Vol. 51722, p. V01AT02A026.
[79] Bonaccorso, F., Cantelli, L., and Muscato, G., 2011, "An Arc Welding Robot Control for a Shaped Metal Deposition Plant: Modular Software Interface and Sensors," IEEE Trans. Ind. Electron., **58**(8), pp. 3126–3132.
[80] Ding, D., Pan, Z., Cuiuri, D., and Li, H., 2015, "A Multi-Bead Overlapping Model for Robotic Wire and Arc Additive Manufacturing (WAAM)," Robot. Comput. Integr. Manuf., **31**, pp. 101–110.
[81] Joosten, S., 2015, "Printing a Stainless Steel Bridge: An Exploration of Structural Properties of Stainless Steel Additive Manufactures for Civil Engineering Purposes," Master's thesis, Delft University of Technology, Delft, Netherlands.
[82] Chen, Y., Zhou, C., and Lao, J., 2011, "A Layerless Additive Manufacturing Process Based on CNC Accumulation," Rapid Prototyp. J., **17**(3), pp. 218–227.
[83] Pan, Y., Zhou, C., Chen, Y., and Partanen, J., 2014, "Multitool and Multi-Axis Computer Numerically Controlled Accumulation for Fabricating Conformal Features on Curved Surfaces," ASME J. Manuf. Sci. Eng., **136**(3), p. 031007.
[84] Stevens, A. G., Oliver, C. R., Kirchmeyer, M., Wu, J., Chin, L., Polsen, E. S., Archer, C., Boyle, C., Garber, J., and Hart, A. J., 2016, "Conformal Robotic Stereolithography," 3D Print. Addit. Manuf., **3**(4), pp. 226–235.
[85] DebRoy, T., Wei, H., Zuback, J., Mukherjee, T., Elmer, J., Milewski, J., Beese, A. M., Wilson-Heid, A., De, A., and Zhang, W., 2018, "Additive Manufacturing of Metallic Components—Process, Structure and Properties," Prog. Mater. Sci., **92**, pp. 112–224.
[86] Liu, Z., Loh, N., Tor, S., and Khor, K., 2002, "Characterization of Powder Injection Molding Feedstock," Mater. Charact., **49**(4), pp. 313–320.
[87] Gonzalez-Gutiérrez, J., Stringari, G. B., and Emri, I., 2012, "Powder Injection Molding of Metal and Ceramic Parts," Some Crit. Issues Injection Molding, pp. 65–88.
[88] Gonzalez-Gutierrez, J., Duretek, I., Kukla, C., Poljšak, A., Bek, M., Emri, I., and Holzer, C., 2016, "Models to Predict' the Viscosity of Metal Injection Molding Feedstock Materials as Function of Their Formulation," Metals, **6**(6), p. 129.
[89] Wu, G., Langrana, N. A., Rangarajan, S., McCuiston, R., Sadanji, R., Danforth, S., and Safari, A., 1999, "Fabrication of Metal Components Using Fdmet: Fused Deposition of Metals," Proceedings of the Solid Freeform Fabrication Symposium, Austin, TX, Aug. 9–11, pp. 775–782.
[90] Geiger, M., Greul, M., Steger, W., and Sindel, M., 1994, "Multiphase Jet Solidification—a New Process Towards Metal Prototypes and a New Data Interface," 1994 International Solid Freeform Fabrication Symposium, Austin, TX, Aug. 8–10, pp. 9–16.
[91] Ruscitti, A., Tapia, C., and Rendtorff, N., 2020, "A Review on Additive Manufacturing of Ceramic Materials Based on Extrusion Processes of Clay Pastes," Ceramica, **66**(380), pp. 354–366.
[92] Kukla, C., Gonzalez-Gutierrez, J., Duretek, I., Schuschnigg, S., and Holzer, C., 2017, "Effect of Particle Size on the Properties of Highly-Filled Polymers for Fused Filament Fabrication," AIP Conf. Proc., **1914**(1), p. 190006.
[93] Bai, Y., and Williams, C. B., 2015, "An Exploration of Binder Jetting of Copper," Rapid Prototyp. J., **21**(2), pp. 177–185
[94] Li, M., Du, W., Elwany, A., Pei, Z., and Ma, C., 2020, "Metal Binder Jetting Additive Manufacturing: A Literature Review," ASME J. Manuf. Sci. Eng., **142**(9), p. 090801.
[95] Appuhamillage, G. A., Chartrain, N., Meenakshisundaram, V., Feller, K. D., Williams, C. B., and Long, T. E., 2019, "110th Anniversary: Vat Photopolymerization-Based Additive Manufacturing: Current Trends and Future Directions in Materials Design," Ind. Eng. Chem. Res., **58**(33), pp. 15109–15118.
[96] Leach, R., and Carmignato, S., 2020, *Precision Metal Additive Manufacturing*, CRC Press, Boca Raton, FL.
[97] Nickels, L., 2018, "Office-Based AM Now Open for Business," Met. Powder Rep., **73**(4), pp. 195–197.
[98] Do, T., Kwon, P., and Shin, C. S., 2017, "Process Development Toward Full-Density Stainless Steel Parts With Binder Jetting Printing," Int. J. Mach. Tools Manuf., **121**, pp. 50–60.
[99] Hagen, D., Kovar, D., Beaman, J., and Gammage, M., 2019, "Laser Flash Sintering for Additive Manufacturing of Ceramics," Tech. Rep., Army Research Lab, Aberdeen Proving Ground, MD.
[100] Gonzalez-Gutierrez, J., Cano, S., Schuschnigg, S., Kukla, C., Sapkota, J., and Holzer, C., 2018, "Additive Manufacturing of Metallic and Ceramic Components by the Material Extrusion of Highly-Filled Polymers: A Review and Future Perspectives," Materials, **11**(5), p. 840.
[101] Wang, J., Shaw, L. L., and Cameron, T. B., 2006, "Solid Freeform Fabrication of Permanent Dental Restorations Via Slurry Micro-Extrusion," J. Am. Ceram. Soc., **89**(1), pp. 346–349.
[102] Hon, K., Li, L., and Hutchings, I., 2008, "Direct Writing Technology—Advances and Developments," CIRP Ann., **57**(2), pp. 601–620.
[103] Pique, A., and Chrisey, D. B., 2001, *Direct-Write Technologies for Rapid Prototyping Applications: Sensors, Electronics, and Integrated Power Sources*, Elsevier, New York.
[104] Mortara, L., Hughes, J., Ramsundar, P. S., Livesey, F., and Probert, D. R., 2009, "Proposed Classification Scheme for Direct Writing Technologies," Rapid Prototyp. J., **15**(4), pp. 299–309.
[105] Lewis, J. A., Smay, J. E., Stuecker, J., and Cesarano, J., 2006, "Direct Ink Writing of Three-Dimensional Ceramic Structures," J. Am. Ceram. Soc., **89**(12), pp. 3599–3609.
[106] Cesarano, J., 1998, "A Review of Robocasting Technology," MRS Online Proc. Libr., **542**(1), pp. 133–139.
[107] Malone, E., and Lipson, H., 2008, "Multi-Material Freeform Fabrication of Active Systems," ASME 2008 9th Biennial Conference on Engineering Systems Design and Analysis, Haifa, Israel, July 7–9, Vol. 48357, pp. 345–353.
[108] Li, B., Roy, T. D., Smith, C., Clark, P., and Church, K. H., 2007, "A Robust True Direct-Print Technology for Tissue Engineering," International Manufacturing Science and Engineering Conference, Atlanta, GA, Oct. 15–18, Vol. 42908, pp. 103–108.
[109] Li, B., Clark, P. A., and Church, K., 2007, "Robust Direct-Write Dispensing Tool and Solutions for Micro/Meso-Scale Manufacturing and Packaging," International Manufacturing Science and Engineering Conference, Atlanta, GA, Oct. 15–18, Vol. 42908, pp. 715–721.
[110] Roman, M. C., Kim, T., Prater, T. J., and Mueller, R. P., 2017, "NASA Centennial Challenge: 3D-Printed Habitat," AIAA SPACE and Astronautics Forum and Exposition, Orlando, FL, Sept. 12–14, p. 5279.
[111] Mueller, R. P., Gelino, N. J., Smith, J. D., Buckles, B. C., Lippitt, T., Schuler, J. M., Nick, A. J., Nugent, M. W., and Townsend, I. I., 2018, "Zero Launch Mass Three-Dimensional Print Head," Proceedings of the 16th Biennial International Conference on Engineering, Science, Construction, and Operations in Challenging Environments, Cleveland, OH, Apr. 9–12, R. B. Malla, ed., American Society of Civil Engineers, Reston, VA, pp. 219–232.
[112] Crump, S. S., 1992, "Apparatus and Method for Creating Three-Dimensional Objects," June 9, U.S. Patent 5,121,329.
[113] Gong, H., Crater, C., Ordonez, A., Ward, C., Waller, M., and Ginn, C., 2018, "Material Properties and Shrinkage of 3D Printing Parts Using Ultrafuse Stainless Steel 316LX Filament," 5th International Conference on Mechanical, Materials and Manufacturing (ICMMM 2018), Orlando, FL, Oct. 13–15, EDP Sciences, Vol. 249, p. 01001.
[114] Turner, B. N., and Gold, S. A., 2015, "A Review of Melt Extrusion Additive Manufacturing Processes: II. Materials, Dimensional Accuracy, and Surface Roughness," Rapid Prototyp. J., **20**(3), pp. 192–204.
[115] Spoerk, M., Gonzalez-Gutierrez, J., Sapkota, J., Schuschnigg, S., and Holzer, C., 2018, "Effect of the Printing Bed Temperature on the Adhesion of Parts Produced by Fused Filament Fabrication," Plast. Rubber Compos., **47**(1), pp. 17–24.
[116] Prater, T., Bean, Q., Werkheiser, N., et al., 2017, "A Ground Based Study on Extruder Standoff Distance for the 3d Printing in Zero *g* Technology Demonstration Mission," Queue for Publication on NASA Technical Reports Server in June.
[117] Dunn, J. J., Hutchison, D. N., Kemmer, A. M., Ellsworth, A. Z., Snyder, M., White, W. B., and Blair, B. R., 2010, "3d Printing in Space: Enabling New Markets and Accelerating the Growth of Orbital Infrastructure," Proc. Space Manuf., **14**, pp. 29–31.
[118] Rahman, K. M., Letcher, T., and Reese, R., 2015, "Mechanical Properties of Additively Manufactured Peek Components Using Fused Filament Fabrication," ASME International Mechanical Engineering Congress and Exposition, Houston, TX, Nov. 13–19, American Society of Mechanical Engineers, Vol. 57359, p. V02AT02A009.
[119] Corman, J., 2014, "Energy and Resource Efficiency of Additive Manufacturing Technologies," PhD thesis, Master's thesis, WZL RWTH Aachen, Germany and MIT, Cambridge, MA.
[120] Goh, G. D., Yap, Y. L., Tan, H., Sing, S. L., Goh, G. L., and Yeong, W. Y., 2020, "Process–Structure–Properties in Polymer Additive Manufacturing Via Material Extrusion: A Review," Crit. Rev. Solid State Mater. Sci., **45**(2), pp. 113–133.
[121] Zaldivar, R., Witkin, D., McLouth, T., Patel, D., Schmitt, K., and Nokes, J., 2017, "Influence of Processing and Orientation Print Effects on the Mechanical and Thermal Behavior of 3d-Printed Ultem® 9085 Material," Addit. Manuf., **13**, pp. 71–80.
[122] Cicala, G., Ognibene, G., Portuesi, S., Blanco, I., Rapisarda, M., Pergolizzi, E., and Recca, G., 2018, "Comparison of Ultem 9085 Used in Fused Deposition Modelling (FDM) With Polytherimide Blends," Materials, **11**(2), p. 285.
[123] Kilroy, J., O'bradaigh, C., and Semprimoschnig, C., 2008, "Mechanical and Physical Evaluation of New Carbon Fibre," SAMPE J., **44**(3), pp. 22–34.
[124] Kuentz, L., Salem, A., Singh, M., Halbig, M., and Salem, J., 2016, "Additive Manufacturing and Characterization of Polylactic Acid (PLA) Composites Containing Metal Reinforcements," https://ntrs.nasa.gov/citations/20160010284.
[125] Murray, B. R., Doyle, A., Feerick, P., Semprimoschnig, C. O., Leen, S. B., and Brádaigh, C. M. Ó., 2017, "Rotational Moulding of Peek Polymer Liners With Carbon Fibre/Peek Over Tape-Placement for Space Cryogenic Fuel Tanks," Mater. Des., **132**, pp. 567–581.
[126] Coughlin, N., Drake, B., Fjerstad, M., Schuster, E., Waege, T., Weerakkody, A., and Letcher, T., 2019, "Development and Mechanical Properties of Basalt Fiber-Reinforced Acrylonitrile Butadiene Styrene for In-Space Manufacturing Applications," J. Compos. Sci., **3**(3), p. 89.

[127] Gallagher, W. R., 2020, "Investigation of Ultem 9085 for Use in Printed Orbital Structures," Master's thesis, Air Force Institute of Technology, Ohio.
[128] Gibson, M. A., Mykulowycz, N. M., Shim, J., Fontana, R., Schmitt, P., Roberts, A., Ketkaew, J., Shao, L., Chen, W., Bordeenithikasem, P., and Myerberg, J. S., 2018, "3d Printing Metals Like Thermoplastics: Fused Filament Fabrication of Metallic Glasses," Mater. Today, **21**(7), pp. 697–702.
[129] Gonzalez-Gutierrez, J., Godec, D., Kukla, C., Schlauf, T., Burkhardt, C., and Holzer, C., 2017, "Shaping, Debinding and Sintering of Steel Components Via Fused Filament Fabrication," 16th International Scientific Conference on Production Engineering – Computer Integrated Manufacturing and High Speed Machining, Zadar, Croatia, June, Vol. 16, p. 99.
[130] Campbell, R., and Wohlers, T., 2017, "Markforged: Taking a Different Approach to Metal Additive Manufacturing," https://repository.lboro.ac.uk/articles/journal_contribution/Markforged_Taking_a_different_approach_to_metal_Additive_Manufacturing/9346493, Accessed July 20, 2021.
[131] Prater, T., Luchinsky, D., Hafiychuk, V., Wheeler, K., Hall, P., Ledbetter, F., Roberts, C., Carey, A., and Flowers, P. F., 2021, "Adaptation of Metal Additive Manufacturing Processes for the International Space Station (ISS)," Society for the Advancement of Material and Process Engineering (SAMPE) neXus 2021, Virtual Event, June 29–July 1, pp. TP21–0000000427.
[132] Crockett, R., Peterson, D., and Cooper, K., 2000, "Fused Deposition Modeling in Microgravity," Proceedings of the Solid Freeform Fabrication Symposium, Austin, TX, Aug. 9–11, pp. 671–678.
[133] Johnston, M. M., Werkheiser, M. J., Cooper, K. G., Snyder, M. P., and Edmunson, J. E., 2014, "3d Printing in Zero-g ISS Technology Demonstration," Tech. Rep.
[134] Cooper, K., and Griffin, M., 2003, "Microgravity Manufacturing Via Fused Deposition." https://ntrs.nasa.gov/citations/20030067856
[135] Cooper, K., McLemore, C., and Anderson, T., 2013, "Cases for Additive Manufacturing on the International Space Station," 50th AIAA Aerospace Sciences Meeting Including the New Horizons Forum and Aerospace Exposition, Nashville, TN, Jan. 9–12, p. 517.
[136] Snyder, M., Dunn, J., and Gonzalez, E., 2013, "The Effects of Microgravity on Extrusion Based Additive Manufacturing," AIAA SPACE 2013 Conference and Exposition, San Diego, CA, Sept. 10–12, p. 5439.
[137] Musso, G., Lentini, G., Enrietti, L., Volpe, C., Ambrosio, E. P., Lorusso, M., Mascetti, G., and Valentini, G., 2016, "Portable on Orbit Printer 3D: 1st European Additive Manufacturing Machine on International Space Station," *Advances in Physical Ergonomics and Human Factors*, R. Goonetilleke and W. Karwowski, eds., Springer, New York, pp. 643–655.
[138] Made In Space Inc., 2016, "Additive Manufacturing Facility (AMF) User Guide," https://madeinspace.us/wp-content/uploads/2019/07/AMFuserguide-1.pdf, Accessed September 4, 2021.
[139] Prater, T., 2015, "Additive Manufacturing: From Rapid Prototyping to Flight."
[140] Werkheiser, M. J., Dunn, J., Snyder, M. P., Edmunson, J., Cooper, K., and Johnston, M. M., 2014, "3d Printing in Zero-g ISS Technology Demonstration," AIAA SPACE 2014 Conference and Exposition, San Diego, CA, Aug. 4–7, p. 4470.
[141] Spivey, R., and Flores, G., 2008, "An Overview of the Microgravity Science Glovebox (MSG) Facility, and the Gravity-Dependent Phenomena Research Performed in the MSG on the International Space Station (ISS)," 46th AIAA Aerospace Sciences Meeting and Exhibit, Reno, NV, Jan. 7–10, p. 812.
[142] Thompson, S. W., Jordan, L. P., and Flores, G. N., 2014, "An Overview of EXPRESS Rack, Microgravity Science Glovebox, and Sub-Rack Facilities for Materials Science Research," https://ntrs.nasa.go v/api/citations/20140010107/downloads/20140010107.pdf, Accessed July 22, 2021.
[143] Prater, T., Bean, Q., Werkheiser, N., Grguel, R., Beshears, R., Rolin, T., Huff, T., Ryan, R., Ledbetter, F., and Ordonez, E., 2017, "Analysis of Specimens From Phase I of the 3d Printing in Zero g Technology Demonstration Mission," Rapid Prototyp. J., **23**(6), pp. 1212–1225.
[144] Prater, T., Bean, Q., Beshears, R., Rolin, T., Werkheiser, N., Ordonez, E., Ryan, R., and Ledbetter, F., III, 2016, "Summary Report on Phase I and Phase II Results from the 3d Printing in Zero-g Technology Demonstration Mission," Vol. I. https://ntrs.nasa.gov/citations/20160008972.
[145] Prater, T., Werkheiser, N., and Ledbetter, F., III, 2018, "Summary Report on Phase I and Phase II Results from the 3d Printing in Zero-g Technology Demonstration Mission," Vol. II. https://ntrs.nasa.gov/citations/20180002403.
[146] Prater, T., Werkheiser, N., Ledbetter, F., Timucin, D., Wheeler, K., and Snyder, M., 2019, "3d Printing in Zero g Technology Demonstration Mission: Complete Experimental Results and Summary of Related Material Modeling Efforts," Int. J. Adv. Manuf. Technol., **101**(1–4), pp. 391–417.
[147] Abeykoon, C., Sri-Amphorn, P., and Fernando, A., 2020, "Optimization of Fused Deposition Modeling Parameters for Improved PLA and ABS 3d Printed Structures," Int. J. Lightweight Mater. Manuf., **3**(3), pp. 284–297.
[148] Leary, M., 2019, *Design for Additive Manufacturing*, Elsevier, New York.
[149] Gong, W., Yifei, L., Tianjin, C., and Ming, L., 2016, "Application of Additive Manufacturing Technology for Space," Chin. J. Space Sci., **36**(4), pp. 571–576.
[150] Cowley, A., Perrin, J., Meurisse, A., Micallef, A., Fateri, M., Rinaldo, L., Bamsey, N., and Sperl, M., 2019, "Effects of Variable Gravity Conditions on Additive Manufacture by Fused Filament Fabrication Using Polylactic Acid Thermoplastic Filament," Addit. Manuf., **28**, pp. 814–820.
[151] Melenka, G. W., Schofield, J. S., Dawson, M. R., and Carey, J. P., 2015, "Evaluation of Dimensional Accuracy and Material Properties of the Makerbot 3d Desktop Printer," Rapid Prototyp. J., **21**(5), pp. 618–627.
[152] Wang, K., 2012, "Die Swell of Complex Polymeric Systems," Viscoelasticity–From Theory to Biological Applications, Juan de Vicente, ed., vol. **1**, pp. 77–96.
[153] Clinton, R. G., Jr., 2017, "NASA Additive Manufacturing Initiatives: In Space Manufacturing and Rocket Engines," https://ntrs.nasa.gov/api/citations/20170009098/downloads/20170009098.pdf, Accessed July 22,2021.
[154] Prater, T., Werkheiser, N., and Ledbetter, F., 2018, "Toward a Multimaterial Fabrication Laboratory: In-Space Manufacturing as an Enabling Technology for Long-Endurance Human Space Flight," https://ntrs.nasa.gov/api/citations/20170012391/downloads/20170012391.pdf, Accessed July 22, 2021.
[155] Lake, R., and Thompson, S., "Conducting Research on the International Space Station Using the Express Rack Facilities," https://ntrs.nasa.gov/citations/20140011636.
[156] Sledd, A., and Mueller, C., 1999, "Express Rack Overview," 37th Aerospace Sciences Meeting and Exhibit, Reno, NV, Jan. 11–14, p. 313.
[157] Thomas, D., Snyder, M. P., Napoli, M., Joyce, E. R., Shestople, P., and Letcher, T., 2017, "Effect of Acrylonitrile Butadiene Styrene Melt Extrusion Additive Manufacturing on Mechanical Performance in Reduced Gravity," AIAA SPACE and Astronautics Forum and Exposition, Orlando, FL, Sept. 12–14, p. 5278.
[158] Prater, T., Werkheiser, N., Ledbetter, F., Wilkerson, M., Soohoo, H., Bean, Q., and Jones, Z., 2017, "NASA's In-Space Manufacturing Project: Materials and Manufacturing Process Development Update," https://ntrs.nasa.gov/api/citations/20170008145/downloads/20170008145.pdf, Accessed July 22, 2021.
[159] Aron, J., 2015, "Print Your Own Satellite—In Space," New Scientist, **227**(3035), pp. 8–9.
[160] Prater, T., 2019, "The Proving Ground: Using Low Earth Orbit as a Test Bed for Manufacturing Technology Development." https://ntrs.nasa.gov/api/citations/20200001003/downloads/20200001003.pdf, Accessed July 22, 2021.
[161] Patane, S., Joyce, E. R., Snyder, M. P., and Shestople, P., 2017, "Archinaut: In-Space Manufacturing and Assembly for Next-Generation Space Habitats," AIAA SPACE and Astronautics Forum and Exposition, Orlando, FL, Sept. 12–14, p. 5227.
[162] Patane, S., Schomer, J., and Snyder, M., 2018, "Design Reference Missions for Archinaut: A Roadmap for In-Space Robotic Manufacturing and Assembly," 2018 AIAA SPACE and Astronautics Forum and Exposition, Orlando, FL, Sept. 17–19, p. 5188.
[163] TechPort, "Archinaut Technology Development," https://techport.nasa.gov/view/93903, Accessed July 20, 2021.
[164] TechPort, "Positrusion Filament Recycling System, Phase I," https://techport.nasa.gov/view/18199, Accessed July 20, 2021.
[165] Cushing, J., Freedman, M., Turner, K., Muhlbauer, R. L., Levedahl, B., Slostad, J., Hoyt, R. P., Kim, T., and Werkheiser, M. J., 2016, "Building a Sustainable In-Space Manufacturing Ecosystem: Positrusion and Crissp," AIAA SPACE 2016, Long Beach, CA, Sept. 13–16, p. 5396.
[166] Risdon, D., 2019, "In-Space Manufacturing (ISM) ISS Refabricator Technology Demonstration," https://ntrs.nasa.gov/api/citations/20190005004/downloads/20190005004.pdf, Accessed July 22, 2021.
[167] Prater, T., Werkheiser, M. J., Ledbetter, F., and Morgan, K., 2018, "In-Space Manufacturing at NASA Marshall Space Flight Center: A Portfolio of Fabrication and Recycling Technology Development for the International Space Station," 2018 AIAA SPACE and Astronautics Forum and Exposition, Orlando, FL, Sept. 17–19, p. 5364.
[168] "In-Space Manufacturing (ISM)," https://ntrs.nasa.gov/api/citations/20190031813/downloads/20190031813.pdf, Accessed July 22, 2021.
[169] Roberts, M., 2018, "International Space Station US National Lab," https://ntrs.nasa.gov/api/citations/20150016175/downloads/20150016175.pdf, Accessed July 10, 2021.
[170] Vellinger, J. C., Boland, E., Kurk, M. A., Milliner, K., and Logan, N. S., 2020, "Biomanufacturing System, Method, and 3D Bioprinting Hardware in a Reduced Gravity Environment," May 19, U.S. Patent 10,655,096.
[171] Vellinger, J. C., Boland, E., Kurk, M. A., Milliner, K., and Logan, N. S., 2020, "Biomanufacturing System, Method, and 3D Bioprinting Hardware in a Reduced Gravity Environment," Dec. 1, U.S. Patent 10,851,333.
[172] Dijksman, J., Pierik, A., Hutchings, I., and Martin, G., 2013, *Inkjet Technology for Digital Fabrication*, Wiley, West Sussex.
[173] Park, J.-U., Hardy, M., Kang, S. J., Barton, K., Adair, K., Lee, C. Y., Strano, M. S., Alleyne, A. G., Georgiadis, J. G., Ferreira, P. M., and Rogers, J. A., 2007, "High-Resolution Electrohydrodynamic Jet Printing," Nat. Mater., **6**(10), pp. 782–789.
[174] Alamán, J., Alicante, R., Peña, J. I., and Sánchez-Somolinos, C., 2016, "Inkjet Printing of Functional Materials for Optical and Photonic Applications," Materials, **9**(11), p. 910.
[175] Haga, M., Maekawa, T., Kuwahara, K., Ohara, A., Kawasak, K., Harada, T., Yoda, S., and Nakamura, T., 1995, "Effect of Electric Field on Marangoni Convection Under Microgravity," J. Jpn. Soc. Microgravity Appl., **12**(1), p. 19.
[176] Edwards, A., Osborne, B., Stoltzfus, J., Howes, T., and Steinberg, T., 2002, "Instabilities and Drop Formation in Cylindrical Liquid Jets in Reduced Gravity," Phys. Fluids, **14**(10), pp. 3432–3438.
[177] Osborne, B. P., and Steinberg, T. A., 2006, "An Experimental Investigation Into Liquid Jetting Modes and Break-Up Mechanisms Conducted in a New Reduced Gravity Facility," Microgravity Sci. Technol., **18**(3), pp. 57–61.
[178] Li, W., Lan, D., and Wang, Y., 2020, "Exploration of Direct-Ink-Write 3d Printing in Space: Droplet Dynamics and Patterns Formation in Microgravity," Microgravity Sci. Technol., **32**(5), pp. 935–940.
[179] Campbell, I., Diegel, O., Kowen, J., and Wohlers, T., 2017, *Wohlers Report 2017 3D Printing and Additive Manufacturing State of the Industry: Annual Worldwide Progress Report*, Wohlers Associates, Fort Collins, CO.

[180] Edwards, P., O'Conner, A., and Ramulu, M., 2013, "Electron Beam Additive Manufacturing of Titanium Components: Properties and Performance," ASME J. Manuf. Sci. Eng., **135**(6), p. 061016.
[181] Gong, X., Anderson, T., and Chou, K., 2012, "Review on Powder-Based Electron Beam Additive Manufacturing Technology," International Symposium on Flexible Automation, St. Louis, MO, June 18–20, American Society of Mechanical Engineers, Vol. 45110, pp. 507–515.
[182] Mani, M., Lane, B. M., Donmez, M. A., Feng, S. C., and Moylan, S. P., 2017, "A Review on Measurement Science Needs for Real-Time Control of Additive Manufacturing Metal Powder Bed Fusion Processes," Int. J. Prod. Res., **55**(5), pp. 1400–1418.
[183] Diegel, O., Singamneni, S., Reay, S., and Withell, A., 2010, "Tools for Sustainable Product Design: Additive Manufacturing," J. Sustain. Develop., **3**(3), pp. 68–75.
[184] Vock, S., Klöden, B., Kirchner, A., Weißgärber, T., and Kieback, B., 2019, "Powders for Powder Bed Fusion: A Review," Prog. Addit. Manuf., **4**(4), pp. 1–15.
[185] Asgari, H., Baxter, C., Hosseinkhani, K., and Mohammadi, M., 2017, "On Microstructure and Mechanical Properties of Additively Manufactured alsi10mg 200c Using Recycled Powder," Mater. Sci. Eng. A, **707**, pp. 148–158.
[186] Park, H. K., Ahn, Y. K., Lee, B. S., Jung, K. H., Lee, C. W., and Kim, H. G., 2017, "Refining Effect of Electron Beam Melting on Additive Manufacturing of Pure Titanium Products," Mater. Lett., **187**, pp. 98–100.
[187] Ardila, L., Garciandia, F., Gonzalez-Díaz, J., Alvarez, P., Echeverria, A., Petite, M., Deffley, R., and Ochoa, J., 2014, "Effect of in718 Recycled Powder Reuse on Properties of Parts Manufactured by Means of Selective Laser Melting," Phys. Procedia, **56**, pp. 99–107.
[188] Brandão, A. D., Gerard, R., Gumpinger, J., Beretta, S., Makaya, A., Pambaguian, L., and Ghidini, T., 2017, "Challenges in Additive Manufacturing of Space Parts: Powder Feedstock Cross-Contamination and Its Impact on End Products," Materials, **10**(5), p. 522.
[189] Santecchia, E., Mengucci, P., Gatto, A., Bassoli, E., Defanti, S., and Barucca, G., 2019, "Cross-Contamination Quantification in Powders for Additive Manufacturing: A Study on Ti-6Al-4V and Maraging Steel," Materials, **12**(15), p. 2342.
[190] Hildreth, O. J., Nassar, A. R., Chasse, K. R., and Simpson, T. W., 2016, "Dissolvable Metal Supports for 3D Direct Metal Printing," 3D Print. Addit. Manuf., **3**(2), pp. 90–97.
[191] Caprio, L., Demir, A. G., Previtali, B., and Colosimo, B. M., 2020, "Determining the Feasible Conditions for Processing Lunar Regolith Simulant Via Laser Powder Bed Fusion," Addit. Manuf., **32**, p. 101029.
[192] Lotz, C., Gerdes, N., Sperling, R., Lazar, S., Linke, S., Neumann, J., Stoll, E., Ertmer, W., and Overmeyer, L., 2020, "Tests of Additive Manufacturing and Other Processes Under Space Gravity Conditions in the Einstein-Elevator," Logist. J. Proc., **2020**, p. 12.
[193] Reitz, B., Lotz, C., Gerdes, N., Linke, S., Olsen, E., Pflieger, K., Sohrt, S., Ernst, M., Taschner, P., Neumann, J., Stoll, E., and Overmeyer, L., 2021, "Additive Manufacturing Under Lunar Gravity and Microgravity," Microgravity Sci. Technol., **33**(2), pp. 1–12.
[194] Zocca, A., Lüchtenborg, J., Mühler, T., Wilbig, J., Mohr, G., Villatte, T., Léonard, F., Nolze, G., Sparenberg, M., Melcher, J., Hilgenberg, K., and Günster, J., 2019, "Enabling the 3D Printing of Metal Components in μ-Gravity," Adv. Mater. Technol., **4**(10), p. 1900506.
[195] Guenster, J., Zocca, A., Gomes, C. M., and Muehler, T., 2017, "Method for Stabilizing a Powder Bed by Means of Vacuum for Additive Manufacturing," Jan. 3, U.S. Patent 9,533,452.
[196] D'Angelo, O., Kuthe, F., Liu, S.-J., Wiedey, R., Bennett, J. M., Meisnar, M., Barnes, A., Kranz, W. T., Voigtmann, T., and Meyer, A., 2021, "A Gravity-Independent Powder-Based Additive Manufacturing Process Tailored for Space Applications," Addit. Manuf., **47**, p. 102349.
[197] Griffith, M., Keicher, D., and Atwood, C. L., 1996, "Free Form Fabrication of Metallic Components Using Laser Engineered Net Shaping (LENS™)," Tech. Rep., Sandia National Labs., Albuquerque, NM.
[198] Keicher, D., Romero, J., Atwood, C., Griffith, M., Jeantette, F., Harwell, L., Greene, D., and Smugeresky, J., 1996, "Laser Engineered Net Shaping (LENS™) for Additive Component Processing," Tech. Rep., Sandia National Labs., Albuquerque, NM.
[199] Dave, V. R., 1996, "Electron Beam (EB)-Assisted Materials Fabrication," Ph.D. thesis, Massachusetts Institute of Technology, Cambridge, MA.
[200] Taminger, K., and Hafley, R. A., 2003, "Electron Beam Freeform Fabrication: A Rapid Metal Deposition Process," https://ntrs.nasa.gov/citations/20040042496.
[201] Stawovy, M. T., 2018, "Comparison of LCAC and PM Mo Deposited Using Sciaky EBAM™," Int. J. Refract. Met. Hard Mater., **73**, pp. 162–167.
[202] Duda, T., and Raghavan, L. V., 2016, "3d Metal Printing Technology," IFAC-PapersOnLine, **49**(29), pp. 103–110.
[203] Wu, B., Pan, Z., Ding, D., Cuiuri, D., Li, H., Xu, J., and Norrish, J., 2018, "A Review of the Wire Arc Additive Manufacturing of Metals: Properties, Defects and Quality Improvement," J. Manuf. Process., **35**, pp. 127–139.
[204] Stecker, S., Lachenberg, K., Wang, H., and Salo, R., 2006, *Advanced Electron Beam Free Form Fabrication Methods & Technology*, AWS Welding Show', Atlanta, GA, pp. 35–46.
[205] Ding, D., Pan, Z., Cuiuri, D., and Li, H., 2015, "Wire-Feed Additive Manufacturing of Metal Components: Technologies, Developments and Future Interests," Int. J. Adv. Manuf. Technol., **81**(1–4), pp. 465–481.
[206] Dass, A., and Moridi, A., 2019, "State of the Art in Directed Energy Deposition: From Additive Manufacturing to Materials Design," Coatings, **9**(7), p. 418.
[207] Gradl, P. R., Protz, C. S., and Wammen, T., 2019, "Additive Manufacturing and Hot-Fire Testing of Liquid Rocket Channel Wall Nozzles Using Blown Powder Directed Energy Deposition Inconel 625 and jbk-75 Alloys," AIAA Propulsion and Energy 2019 Forum, Indianapolis, IN, Aug. 19–22, p. 4362.
[208] Gradl, P. R., Protz, C. S., Zagorski, K., Doshi, V., and McCallum, H., "Additive Manufacturing and Hot-Fire Testing of Bimetallic Grcop-84 and c-18150 Channel-Cooled Combustion Chambers Using Powder Bed Fusion and Inconel 625 Hybrid Directed Energy Deposition," AIAA Propulsion and Energy 2019 Forum, Indianapolis, IN, Aug. 19–22, p. 4390.
[209] Naden, N., and Prater, T., 2020, "A Review of Welding In Space and Related Technologies," https://ntrs.nasa.gov/citations/20200002259.
[210] Liu, X., Dong, Q., Wang, P., and Chen, H., 2021, "Review of Electron Beam Welding Technology in Space Environment," Optik, **225**, p. 165720.
[211] Kuntanapreeda, S., and Hess, D., 2021, "Opening Access to Space by Maximizing Utilization of 3d Printing in Launch Vehicle Design and Production," Appl. Sci. Eng. Prog., **14**(2), pp. 143–145.
[212] Lee, K.-O., Lim, B., Kim, D.-J., Hong, M., and Lee, K., 2020, "Technology Trends in Additively Manufactured Small Rocket Engines for Launcher Applications," J. Korean Soc. Propul. Eng., **24**(2), pp. 73–82.
[213] Balla, V. K., Roberson, L. B., O'Connor, G. W., Trigwell, S., Bose, S., and Bandyopadhyay, A., 2012, "First Demonstration on Direct Laser Fabrication of Lunar Regolith Parts," Rapid Prototyp. J., **18**(6), pp. 451–457.
[214] Martina, F., Ding, J., Williams, S., Caballero, A., Pardal, G., and Quintino, L., 2019, "Tandem Metal Inert Gas Process for High Productivity Wire Arc Additive Manufacturing in Stainless Steel," Addit. Manuf., **25**, pp. 545–550.
[215] Martina, F., Williams, S. W., and Colegrove, P. A., 2013, "Improved Microstructure and Increased Mechanical Properties of Additive Manufacture Produced Ti-6Al-4V by Interpass Cold Rolling,"2013 International Solid Freeform Fabrication Symposium, Austin, TX, Aug. 12–14, pp. 490–496.
[216] Colegrove, P., McAndrew, A., Ding, J., Martina, F., Kurzynski, P., and Williams, S., 2016, "System Architectures for Large Scale Wire+ Arc Additive Manufacture," 10th International Conference on Trends in Welding Research, Tokyo, Japan, Oct. 11–14, p. 5.
[217] Taminger, K., Hafley, R. A., and Dicus, D. L., 2002, "Solid Freeform Fabrication: An Enabling Technology for Future Space Missions," https://ntrs.nasa.gov/citations/20030013635.
[218] Watson, J., Taminger, K., Hafley, R., and Petersen, D., 2002, "Development of a Prototype Low-Voltage Electron Beam Freeform Fabrication System," 2002 International Solid Freeform Fabrication Symposium, Austin, TX, Aug. 5–7, pp. 458–465.
[219] Taminger, K. M., and Hafley, R. A., 2006, "Electron Beam Freeform Fabrication for Cost Effective Near-Net Shape Manufacturing," https://ntrs.nasa.gov/citations/20080013538
[220] Hafley, R., Taminger, K., and Bird, R., 2007. "Electron Beam Freeform Fabrication in the Space Environment," 45th AIAA Aerospace Sciences Meeting and Exhibit, Reno, NV, Jan. 8–11, p. 1154.
[221] Wallace, T. A., Bey, K. S., Taminger, K. M., and Hafley, R. A., 2004, "A Design of Experiments Approach Defining the Relationships Between Processing and Microstructure for Ti-6Al-4V," 2004 International Solid Freeform Fabrication Symposium, Austin, TX, Aug. 2–4, pp. 104–115.
[222] Taminger, K., and Hafley, R. A., 2002, "Characterization of 2219 Aluminum Produced by Electron Beam Freeform Fabrication," 2002 International Solid Freeform Fabrication Symposium, Austin, TX, Aug. 5–7, pp. 482–489.
[223] Taminger, K., Hafley, R. A., Fahringer, D. T., and Martin, R. E., 2004, "Effect of Surface Treatments on Electron Beam Freeform Fabricated Aluminum Structures," 2004 International Solid Freeform Fabrication Symposium, Austin, TX, Aug. 2–4, pp. 460–470.
[224] Taminger, K. M., 2008, "Electron Beam Freeform Fabrication: A Fabrication Process That Revolutionizes Aircraft Structural Designs and Spacecraft Supportability," https://ntrs.nasa.gov/citations/20080021301.
[225] Gockel, J., Beuth, J., and Taminger, K., 2014, "Integrated Control of Solidification Microstructure and Melt Pool Dimensions in Electron Beam Wire Feed Additive Manufacturing of Ti-6Al-4V," Addit. Manuf., **1**, pp. 119–126.
[226] Pugh, A., Billing, C., Bevan, R., Green, A., Kitsos, T., Brittain, B., Schwarz, J., Bramley, S., and Moore, J., 2021, "The West Midlands Space Cluster Development Programme: University Asset Mapping," University of Birmingham Executive Report, March 31, 2021, p. 12. https://www.birmingham.ac.uk/documents/college-social-sciences/business/research/city-redi/space-cluster/wm-space-cluster-asset-mapping.pdf.
[227] Molitch-Hou, M., 2016, "Researchers 3D Print Metal in Zero G for ESA," https://www.engineering.com/story/researchers-3d-print-metal-in-zero-g-for-esa, Accessed June 13, 2021.
[228] Gu, H., and Li, L., 2019, "Computational Fluid Dynamic Simulation of Gravity and Pressure Effects in Laser Metal Deposition for Potential Additive Manufacturing in Space," Int. J. Heat Mass Transfer, **140**, pp. 51–65.
[229] Xie, H., Duan, X., Wang, G., Fan, S., and Ding, X., 2019, "Liquid Bridge Simulation of Metal-Wire Laser Additive Manufacturing in Microgravity Environment," 9th International Symposium on Advanced Optical Manufacturing and Testing Technologies: Subdiffraction-Limited Plasmonic Lithography and Innovative Manufacturing Technology, Chengdu, China, June 26–29, International Society for Optics and Photonics, Vol. 10842, p. 108420O.
[230] Clarinval, A.-M., 2006, "Production of Metallic and Ceramic Parts With the Optoform Process," Tech. Rep., Centre De Recherches Scientifiques Et Techniques De L'industrie Fabrications.

[231] Liu, M., Tang, W., Duan, W., Li, S., Dou, R., Wang, G., Liu, B., and Wang, L., 2019, "Digital Light Processing of Lunar Regolith Structures With High Mechanical Properties," Ceram. Int., **45**(5), pp. 5829–5836.
[232] Cheibas, I., Laot, M., Popovich, V., Rich, B., and Castillo, S. R., "Additive Manufacturing of Functionally Graded Materials With In-Situ Resources," Technical Report, ESA.
[233] Dou, R., Tang, W. Z., Wang, L., Li, S., Duan, W. Y., Liu, M., Zhang, Y. B., and Wang, G., 2019, "Sintering of Lunar Regolith Structures Fabricated Via Digital Light Processing," Ceram. Int., **45**(14), pp. 17210–17215.
[234] Space, M. I., 2017, "New Space-Based Manufacturing Technologies Demonstrated by Made In Space," https://medium.com/made-in-space/new-space-based-manufacturing-technologies-demonstrated-by-made-in-space-79000e771ac4, Feb., Accessed July 10,2021.
[235] Moore, S., 2021, "The Future of 3d Printing Ceramics In Space," https://www.azom.com/article.aspx?ArticleID=20024, Jan., Accessed July 10, 2021.
[236] Dou, R., Tang, W., Hu, K., and Wang, L., 2022, "Ceramic Paste for Space Stereolithography 3d Printing Technology in Microgravity Environment," J. Eur. Ceram. Soc., **42**(9), pp. 3968–3975.
[237] Cross, M. M., 1965, "Rheology of Non-Newtonian Fluids: A New Flow Equation for Pseudoplastic Systems," J. Colloid Sci., **20**(5), pp. 417–437.
[238] Dini, E., 2009, "D-Shape-the 21st Century Revolution in Building Technology Has a Name," London, pp. 1–16.
[239] Cesaretti, G., 2012, "3d Printed Building Blocks Using Lunar Soil-final report (3dp-alt-rp-0001)". European Space Agency, ALTA, May 2012, 31. Document No. 3DP-ALT-ES1 0001.
[240] Cesaretti, G., Dini, E., De Kestelier, X., Colla, V., and Pambaguian, L., 2014, "Building Components for an Outpost on the Lunar Soil by Means of a Novel 3d Printing Technology," Acta Astronaut., **93**, pp. 430–450.
[241] Feuerbacher, B., Hamacher, H., and Naumann, R. J., 2012, *Materials Sciences In Space: A Contribution to the Scientific Basis of Space Processing*, Springer, Berlin.
[242] Snyder, M., Napoli, M., Dunn, J., and Kemmer, A., 2015, "Metal Casting Methods in Microgravity and Other Environments," May 28, U.S. Patent Ap. 14/555,234.
[243] Wang, G., Zhao, W., Liu, Y., and Cheng, T., 2020, "Review of Space Manufacturing Technique and Developments," Sci. Sin.: Phys. Mech. Astron., **50**(4), p. 047006.
[244] Vincent, G., 2003, "Machining in Microgravity," AIP Conf. Proc., **654**, pp. 882–886.
[245] Zhu, Z., Dhokia, V. G., Nassehi, A., and Newman, S. T., 2013, "A Review of Hybrid Manufacturing Processes—State of the Art and Future Perspectives," Int. J. Comput. Integr. Manuf., **26**(7), pp. 596–615.
[246] Merklein, M., Junker, D., Schaub, A., and Neubauer, F., 2016, "Hybrid Additive Manufacturing Technologies—An Analysis Regarding Potentials and Applications," Phys. Procedia, **83**, pp. 549–559.
[247] Chong, L., Ramakrishna, S., and Singh, S., 2018, "A Review of Digital Manufacturing-Based Hybrid Additive Manufacturing Processes," Int. J. Adv. Manuf. Technol., **95**(5), pp. 2281–2300.
[248] Prater, T. J., Werkheiser, M. J., Jehle, A., Ledbetter, F., Bean, Q., Wilkerson, M., Soohoo, H., and Hipp, B., 2017, "NASA's In-Space Manufacturing Project: Development of a Multimaterial Fabrication Laboratory for the International Space Station," AIAA SPACE and Astronautics Forum and Exposition, Orlando, FL, Sept. 12–14, p. 5277.
[249] Prater, T., Edmunson, J., Ledbetter, F., Fiske, M., Hill, C., Meyyappan, M., Roberts, C., Huebner, L., Hall, P., and Werkheiser, N., 2019, "NASA's In-Space Manufacturing Project: Update on Manufacturing Technologies and Materials to Enable More Sustainable and Safer Exploration," 70th International Astronautical Congress (IAC), Washington, DC, Oct. 21–25, pp. IAC–19.D3.2B.5.
[250] Grace, R., 2017, "One of NASA's Missions: Taking 3D Printing to New Heights: In-Space Manufacturing, Despite Many Challenges, Offers the Potential to Enhance Astronaut Safety, Lighten Payloads & Extend Missions," Plast. Eng., **73**(8), pp. 8–15.
[251] Warner, C., 2017, "NASA Selects Three Companies to Develop 'FabLab' Prototypes," https://www.nasa.gov/press-release/nasa-selects-three-companies-to-develop-fablab-prototypes, Accessed July 24, 2021.
[252] Nickels, L., 2016, "Additive Manufacturing: A user's Guide," Metal Powder Report, **71**(2), pp. 100–105.
[253] Levy, A., Miriyev, A., Sridharan, N., Han, T., Tuval, E., Babu, S. S., Dapino, M. J., and Frage, N., 2018, "Ultrasonic Additive Manufacturing of Steel: Method, Post-Processing Treatments and Properties," J. Mater. Process. Technol., **256**, pp. 183–189.
[254] Ram, G. J., Robinson, C., Yang, Y., and Stucker, B., 2007, "Use of Ultrasonic Consolidation for Fabrication of Multimaterial Structures," Rapid Prototyp. J., **13**(4), pp. 226–235.
[255] Obielodan, J., and Stucker, B., 2010, "Dual-Material Minimum Weight Structures Fabrication Using Ultrasonic Consolidation," 21st Annual International Solid Freeform Fabrication Symposium, Austin, TX, Aug. 9–11, pp. 48–81.
[256] Hehr, A., and Norfolk, M., 2019, "A Comprehensive Review of Ultrasonic Additive Manufacturing," Rapid Prototyp. J., **26**(3), pp. 445–458.
[257] Robinson, C. J., Stucker, B., Lopes, A. J., Wicker, R., and Palmer, J. A., 2006, "Integration of Direct-Write (DW) and Ultrasonic Consolidation (UC) Technologies to Create Advanced Structures With Embedded Electrical Circuitry," 2006 International Solid Freeform Fabrication Symposium, Austin, TX, Aug. 14–16, pp. 60–69.
[258] Siggard, E. J., Madhusoodanan, A. S., Stucker, B., and Eames, B., 2006, "Structurally Embedded Electrical Systems Using Ultrasonic Consolidation (UC)," 2006 International Solid Freeform Fabrication Symposium, Austin, TX, Aug. 14–16, pp. 70–83.
[259] Hernandez, L. A., and Stucker, B., 2009, *Integration & Process Planning for Combined Ultrasonic Consolidation and Direct Write*, Utah State University, Logan.
[260] Prater, T., Werkheiser, N., Morgan, K., and Ledbetter, F., 2018, "The High Frontier: A New Age of Manufacturing In Space," https://ntrs.nasa.gov/api/citations/20180007963/downloads/20180007963.pdf, Accessed July 22, 2021.
[261] Prater, T., Edmunson, J., Ledbetter, F. E., Wheeler, K. R., Hafiychuk, V., Fiske, M., and Elrod, L., 2019, "Overview of the In-Space Manufacturing Technology Portfolio."
[262] TechPort, "Sintered Inductive Metal Printer With Laser Exposure, Phase I," https://techport.nasa.gov/view/89677, Accessed July 20, 2021.
[263] Kurk, A., 2017, "Sintered Inductive Metal Printer With Laser Enhancement," Proceedings of the National Space and Missile Materials Symposium, Palm Springs, CA, June 26–29.
[264] TechPort, "Sintered Inductive Metal Printer With Laser Exposure, Phase II," https://techport.nasa.gov/view/93762, Accessed July 20, 2021.
[265] TechPort, "Metal Advanced Manufacturing Bot-Assisted Assembly (MAMBA) Process, Phase I," https://techport.nasa.gov/view/93631, Accessed July 20, 2021.
[266] Muhlbauer, R., 2017, *Metal Advanced Manufacturing Bot Assembly (MAMBA) Process*, Small Business Innovative Research (SBIR) Abstract. https://sbir.nasa.gov/SBIR/abstracts/17/sbir/phase1/SBIR-17-1-H7.02-9710.html Accessed July 20, 2021.
[267] TechPort, "Metal Advanced Manufacturing Bot-Assisted Assembly (MAMBA) Process, Phase II," https://techport.nasa.gov/view/101899, Accessed July 20, 2021.
[268] TechPort, "The Vulcan Advanced Hybrid Manufacturing System, Phase I," https://techport.nasa.gov/view/93797, Accessed July 20, 2021.
[269] TechPort, "The Vulcan Advanced Hybrid Manufacturing System, Phase II," https://techport.nasa.gov/view/101817, Accessed July 20, 2021.
[270] Singh, P., 2020, "Materials-Processing Relationships for Metal Fused Filament Fabrication of Ti-6Al-4V Alloy," PhD thesis, University of Louisville, KY.
[271] Luchinsky, D. G., Hafiychuk, V., Wheeler, K. R., and Prater, T. J., 2021, "Analysis of Nonlinear Shrinkage for the Bound Metal Deposition Manufacturing Using Multi-Scale Approach," Tech. Rep.
[272] Zubrin, R., 2011, *Case for Mars*, Simon and Schuster, New York.
[273] Voorhies, A. A., Ott, C. M., Mehta, S., Pierson, D. L., Crucian, B. E., Feiveson, A., Oubre, C. M., Torralba, M., Moncera, K., Zhang, Y., and Zurek, E., 2019, "Study of the Impact of Long-Duration Space Missions at the International Space Station on the Astronaut Microbiome," Sci. Rep., **9**(1), pp. 1–17.
[274] Sobel, A., 2020, "Update on Bioprinting and Biofabrication in Support of Aerospace Missions and the Human Condition," Aerosp. Med. Hum. Perform., **91**(5), pp. 457–458.
[275] Hospodiuk, M., Dey, M., Sosnoski, D., and Ozbolat, I. T., 2017, "The Bioink: A Comprehensive Review on Bioprintable Materials," Biotechnol. Adv., **35**(2), pp. 217–239.
[276] Mandrycky, C., Wang, Z., Kim, K., and Kim, D.-H., 2016, "3d Bioprinting for Engineering Complex Tissues," Biotechnol. Adv., **34**(4), pp. 422–434.
[277] Dababneh, A. B., and Ozbolat, I. T., 2014, "Bioprinting Technology: A Current State-of-the-Art Review," ASME J. Manuf. Sci. Eng., **136**(6), p. 061016.
[278] Gungor-Ozkerim, P. S., Inci, I., Zhang, Y. S., Khademhosseini, A., and Dokmeci, M. R., 2018, "Bioinks for 3D Bioprinting: An Overview," Biomater. Sci., **6**(5), pp. 915–946.
[279] Parfenov, V. A., Khesuani, Y. D., Petrov, S. V., Karalkin, P. A., Koudan, E. V., Nezhurina, E. K., Pereira, F. D., Krokhmal, A. A., Gryadunova, A. A., Bulanova, E. A., and Vakhrushev, I. V., 2020, "Magnetic Levitational Bioassembly of 3d Tissue Construct in Space," Sci. Adv., **6**(29), p. eaba4174.
[280] Short, K., and Van Buren, D., 2014, "Printable Spacecraft: Flexible Electronic Platforms for NASA Missions" [Final Report: Early Stage Innovation, NASA Innovative Advanced Concepts (NIAC) Phase 2].
[281] Meyyappan, M., Koehne, J. E., and Han, J.-W., 2015, "Nanoelectronics and Nanosensors for Space Exploration," MRS Bull., **40**(10), pp. 822–828.
[282] Han, J.-W., Kim, B., Li, J., and Meyyappan, M., 2012, "Carbon Nanotube Based Humidity Sensor on Cellulose Paper," J. Phys. Chem. C, **116**(41), pp. 22094–22097.
[283] Han, J.-W., Kim, B., Li, J., and Meyyappan, M., 2013, "A Carbon Nanotube Based Ammonia Sensor on Cotton Textile," Appl. Phys. Lett., **102**(19), p. 193104.
[284] Han, J.-W., Kim, B., Li, J., and Meyyappan, M., 2014, "A Carbon Nanotube Based Ammonia Sensor on Cellulose Paper," RSC Adv., **4**(2), pp. 549–553.
[285] Kim, B., Lu, Y., Kim, T., Han, J.-W., Meyyappan, M., and Li, J., 2014, "Carbon Nanotube Coated Paper Sensor for Damage Diagnosis," ACS Nano, **8**(12), pp. 12092–12097.
[286] Seol, M.-L., Han, J.-W., Moon, D.-I., and Meyyappan, M., 2017, "Triboelectric Nanogenerator for Mars Environment," Nano Energy, **39**, pp. 238–244.
[287] Seol, M.-L., Han, J.-W., Moon, D.-I., Yoon, K. J., Hwang, C. S., and Meyyappan, M., 2018, "All-Printed Triboelectric Nanogenerator," Nano Energy, **44**, pp. 82–88.
[288] Wilkinson, N., Smith, M., Kay, R., and Harris, R., 2019, "A Review of Aerosol Jet Printing—A Non-Traditional Hybrid Process for Micro-Manufacturing," Int. J. Adv. Manuf. Technol., **105**(11), pp. 4599–4619.

[289] Wu, C.-H., and Thompson, F. V., 2017, "Application of Temperature-Controlled Thermal Atomization for Printing Electronics In Space," Marshall Space Flight Center Faculty Fellowship Program, p. 197.
[290] TechPort, "Adaptive Laser Sintering System for In-Space Printed Electronics, Phase I," https://techport.nas a.gov/view/93332, Accessed July 20, 2021.
[291] Renn, M. J., Schrandt, M., Renn, J., and Feng, J. Q., 2017, "Localized Laser Sintering of Metal Nanoparticle Inks Printed With Aerosol Jet® Technology for Flexible Electronics," J. Microelectron. Electron. Packag., **14**(4), pp. 132–139.
[292] TechPort, "Plasma Jet Printing Technology for In-Space Manufacturing and In-Situ Resource Utilization, Phase I," https://techport.nasa.gov/view/94708, Accessed July 20, 2021.
[293] Perez, K. B., and Williams, C. B., 2013, "Combining Additive Manufacturing and Direct Write for Integrated Electronics—A Review," 24th International Solid Freeform Fabrication Symposium—An Additive Manufacturing Conference, SFF, Austin, TX, Aug. 12–14, pp. 962–979.
[294] Marshall, W. M., Stegeman, J. D., Zemba, M., MacDonald, E., Shemelya, C., Wicker, R., Kwas, A., and Kief, C., 2015, "Using Additive Manufacturing to Print a Cubesat Propulsion System," 51st AIAA/SAE/ASEE Joint Propulsion Conference, Orlando, FL, July 27–29, p. 4184.
[295] Shemelya, C., Cedillos, F., Aguilera, E., Espalin, D., Muse, D., Wicker, R., and MacDonald, E., 2014, "Encapsulated Copper Wire and Copper Mesh Capacitive Sensing for 3-d Printing Applications," IEEE Sens. J., **15**(2), pp. 1280–1286.
[296] Mitra, D., Striker, R., Cleveland, J., Braaten, B. D., Kabir, K. S., Aqueeb, A., Burczek, E., Roy, S., and Ye, S., 2021, "A 3D Printed Microstrip Patch Antenna Using Electrifi Filament for In-Space Manufacturing," 2021 United States National Committee of URSI National Radio Science Meeting (USNC-URSI NRSM), Boulder, CO, Jan. 4–9, IEEE, pp. 216–217.
[297] Guthrie, P., 2016, "Sporks in Space: Bothell Firm Brings Recycling to Final Frontier," Herald Bus. J., **24**.
[298] Prater, T., Tilson, W., and Jones, Z., 2015, "Characterization of Machine Variability and Progressive Heat Treatment in Selective Laser Melting of Inconel 718," JANNAF Propulsion Meeting, No. M15-4523.
[299] Spivey, R., Gilley, S., Ostrogorsky, A., Grugel, R., Smith, G., and Luz, P., 2003, "SUBSA and PFMI Transparent Furnace Systems Currently in Use in the International Space Station Microgravity Science Glovebox," 41st Aerospace Sciences Meeting and Exhibit, Reno, NV, Jan. 6–9, p. 1362.